NTNU
Norwegian University of
Science and Technology

A Parametric Study of Dynamic Response in Numerical Pantograph-Catenary Interaction Model

Håkon Elvsaas

Civil and Environmental Engineering
Submission date: May 2018
Supervisor: Anders Rönnquist, KT
Co-supervisor: Petter Nåvik, KT

Norwegian University of Science and Technology
Department of Structural Engineering

Abstract

The dynamic interaction between catenary system and pantograph is of importance to anyone seeking to facilitate higher railway speed. A combination of live measurements being costly and the large amount of computational power available, has encouraged the use of numerical simulation to examine this field. Through this thesis, the target has been to develop a functional numerical model, able to analyse the dynamic response due to contact, and produce credible data. After comparing simulated results to benchmark values, the impact of two different model features; namely the cant height and overlap section, has been investigated.

Sammendrag

For å være i stand til å øke hastigheten på både dagens og fremtidens jernbaner, er det viktig å tilegne seg kunnskap om samspillet mellom pantograf og kontaktledningsanlegg. Siden kostnadene knyttet til måling og testing i full skala er høye, og tilgangen til datakraft stadig øker, har numerisk simulering blitt et nyttig verktøy når det kommer til nettopp dette. I denne oppgaven har målet vært å utvikle en allsidig kode for kontaktsimulering ved bruk av det elementmetode-baserte programmet ABAQUS. Etter å ha kontrollert at den resulterende modellen er i stand til å gjengi realistiske verdier, har innvirkningen av å inkludere overhøyde og vekslingsfelt blitt undersøkt nærmere.

Acknowledgments

I would like to thank both my supervisor Anders Rønnquist and co-Supervisor Petter Nåvik for providing a challenging, yet interesting, assignment, and for guidance and advice. Also, without the access to extra computational power, this thesis would still be near the starting point.
A shout-out to all my friends and flatmates through the years here in Trondheim.

Contents

List of Figures

List of Tables

Abbreviations

OCS	=	Overhead Contact Line System
OCL	=	Overhead Contact Line
CW	=	Contact Wire
MW	=	Messenger Wire
CA	=	Catenary Wire
AC	=	Alternating Current
DC	=	Direct Current
FEM	=	Finite Element Method
FEA	=	Finite Element Analysis
DOF	=	Degree Of Freedom
TSI	=	Technical Specifications for Interoperability
CAE	=	Complete Abaqus Environment

Chapter 1

Introduction

Electrified railway transportation is expected to play an important role in the coming years, as focus is shifted towards being more environmentally-friendly. In order for train transport to compete with other means of transportation, such as air transport, the duration of travel should be minimised, and much research focuses on how to solve this. Since the propulsion of modern trains is obtained through the mechanical contact between pantograph and contact wire, it is critical to maintain this contact. It is also desirable to limit the force to some degree, as excessive force will result in unnecessary wear for both contact wire and pantograph. When the speed is increased, the response of the complex catenary system is difficult to predict, however approximated solutions can be found through numerical simulations. The aim of this thesis is to develop a code suitable for numerical simulation of interaction between pantograph and catenary system. It should include the possibility to alter a large range of parameters, and also allow for this to be done in an easy and intuitive way. When the code is functioning, it should be available as a tool to investigate both the impact of cant height inclusion in the model, and how overlap sections affect forces and displacements.
The text is structured in the following way:

- **Chapter 2:** Description of the catenary system, pantograph and relevant expressions
- **Chapter 3:** Theory is presented
- **Chapter 4:** Description of the numerical model. The chapter also addresses challenges related to numerical modelling
- **Chapter 5:** Results and discussion

Chapter 2

System description

The main function of an overhead contact line system (OCS) is to provide electricity to the train in a reliable way. Because of difference in design speed, track geometry, power supply (AC/DC), etc., these systems come in a wide range of designs. However, they mostly consist of a contact wire, at least one catenary wire, droppers, poles/masts and brackets. A simplified OCS is shown in figure 2.1. An explanation of the vital parts is given in the following section. Table 2.1 shows materials and profiles for some of the systems being used in Norway today. In addition to these, older systems, such as table 54, are still in use.

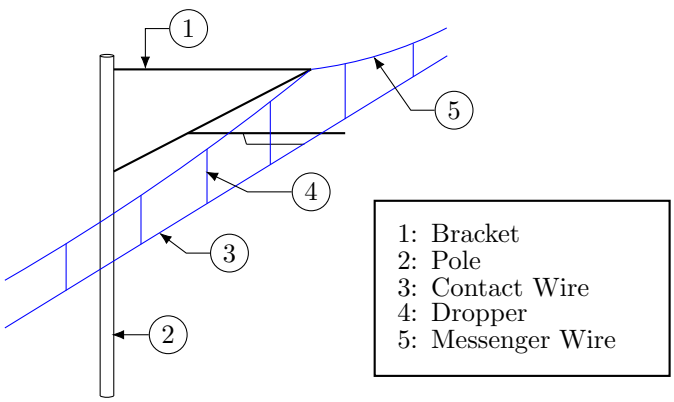

Figure 2.1: Part of an OCL system

Table 2.1: Overhead Contact Line Systems currently installed in Norway

System	Contact Wire	Catenary Wire	Dropper Wire	Stitched?
System 25	AC-120,CuAg0.1	BzII,70/19	BzII,10/49	Yes
System 20	AC-100,CuAg0.1	BzII,50/19	BzII,10/49	Yes
System 35	AC-100,Cu-ETP	Cu-ETP,50/7	Cu-ETP 10/49	Yes

2.1 OCS components

The overhead line system comprises contact wire, catenary wire, droppers, stitch wires and tensioning devices. An overhead line section is subdivided into multiple spans of different lengths, and possibly of different design. A simple overhead contact line(OCL) design, made up of a contact wire, messenger wire and droppers in between, is shown in figure 2.2.

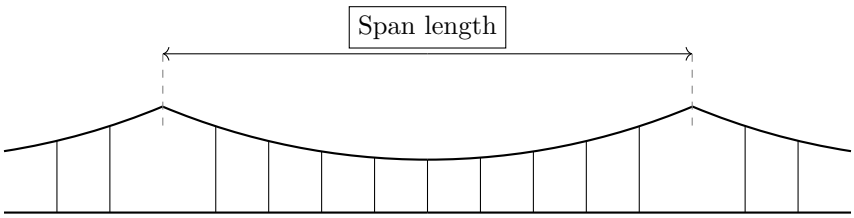

Figure 2.2: OCL span seen from the side

2.1.1 Contact Wire

The contact wire is, like the name suggests, the wire that is in contact with the pantograph. Since the wire conducts electricity, it must be made out of a material with high electrical conductivity. Frictional forces between wire and pantograph will cause damage over time, and the material should be able to withstand mechanical wear in a satisfactory manner. Copper alloys fit these requirements well, and can also be made at a relative low cost, and equipped with a sufficient resistance against corrosion. The contact wires are held in place by several clips, and the profile is therefore grooved. The design of these profiles are standardised. For contact wires made out of copper or copper alloys, dimensions can be found in EN 50149. A BC-100 profile would refer to a profile of type B, with a circular shape and a cross-sectional area of 100 mm^2. Figure 2.3 shows such a profile.

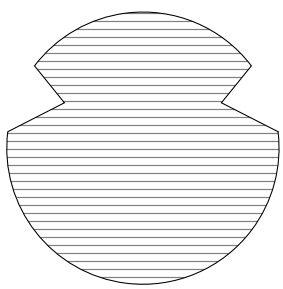

Figure 2.3: A BC-100 profile (dimensions left out)

2.1.2 Catenary Wire

The catenary wire, also referred to as the messenger wire, supports the contact wire through the droppers. Wire systems designed for relatively low speed, such as those compatible with trolleybuses, do not necessarily facilitate catenary wires. For railroad application, where higher speeds are expected, using only a contact wire would cause too large displacements. Since the catenary wire is not exposed to any direct contact, stranded conductors can be utilised. As for the contact wire, copper alloys are often preferred, much for the same reasons. From table 2.1 it can be seen that system 20 is installed with a BZII,50/19 catenary wire. This means that the wire is made out of a bronze alloy, and that the profile has a nominal area of 50 mm^2, consisting of 19 strands (see fig 2.4). Some of the key characteristics of the catenary wire heavily influence the response of the whole system, as will be explained later on.

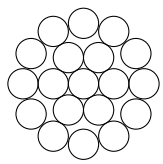

Figure 2.4: 19-strand wire profile

2.1.3 Droppers

The droppers act as a link between the contact wire and the catenary wire or stitch wire. They come in a variety of designs, depending on what functionality that is required (adjustable, current carrying, etc.). It is important to control the contact wire height along the spans, and this is done through adjustment of dropper lengths. This is typically tabulated data, where the dropper lengths to be used depend on span lengths, tension in the contact and catenary wire, number of droppers to be used, etc.. The droppers are attached to the wires by dropper clips. Figure 2.5 shows a basic dropper design.

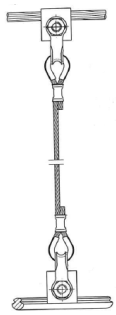

Figure 2.5: A non-current carrying dropper[16]

2.1.4 Stitch Wire

To make the elasticity more equally distributed over the span length, a stitch wire can be installed (figure 2.6b).The addition of this wire improves the performance of the OCL, and is used in most modern sections, especially sections designed for high-speed. The compound catenary system, which features an extra support wire, is another alternative that helps decreasing the variation in elasticity.

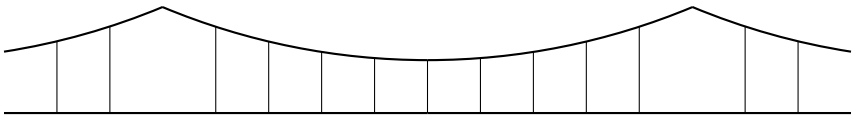

(a) Basic design

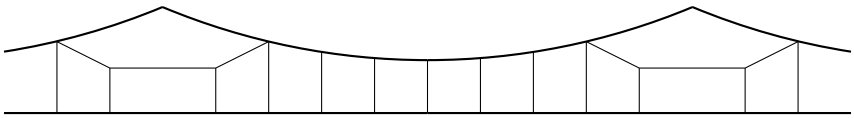

(b) stitched design

Figure 2.6: Different OCL designs

2.1.5 Brackets and poles

Cantilevers mounted to poles is the most common support for the OCL. These can vary in design, but the main parts remain the same. Figure 2.7 shows a cantilever, and the name of the most vital parts. The catenary wire is attached to the top anchor, while the contact wire is attached to the steady arm. This light-weight steady arm is allowed to move in vertical direction, but must be able to withstand the lateral forces that occur due to stagger. Excessive upwards displacements should be limited in order to avoid collision between steady arm and the registration arm above.

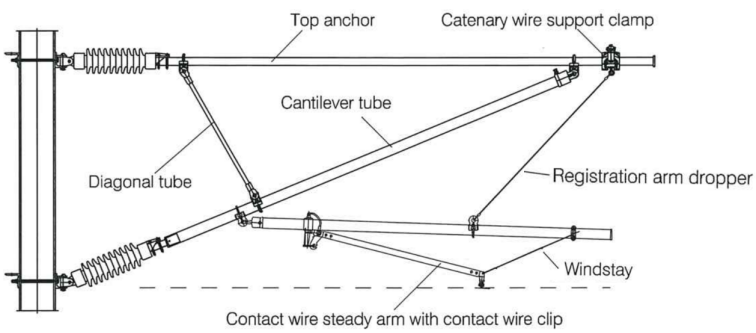

Figure 2.7: Hinged cantilever design [16]

The bracket must be designed as either a pull-off support or a push-off support, as depicted in figure 2.8. The difference between these two lies in the orientation of the contact wire steady arm. Due to the stagger of the contact line, this arm is oriented so that it is in tension, rather than compression.

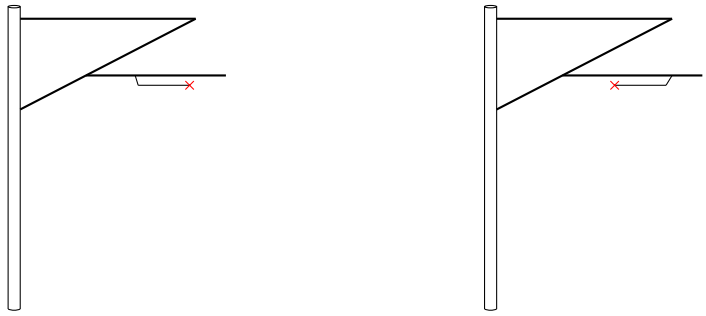

(a) Pull-off support **(b)** Push-off support

Figure 2.8: Cantilever configurations

2.2 The Pantograph

The pantograph is the device mounted on top of the train, permitting current collection from the contact line. It consists of a collector head, an articulating arm and a frame attached to the car body. Figure 2.9 allows for a more detailed examination of the pantograph. Connection with the contact wire is made through carbon strips. These strips are able to conduct electricity, and at the same time function as dry lubricant, reducing wear compared to a pure metal connection. In the long run, wear to both pantograph and contact wire does occur, and the strips are therefore replaceable. The vertical position of the pantograph is usually controlled by a pneumatic system, making the static contact force adjustable.

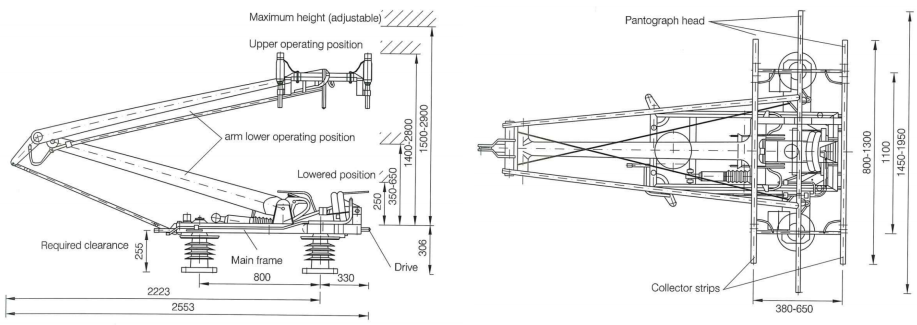

(a) Side view **(b)** Top view

Figure 2.9: Pantograph of type DSA-350 S [16]

2.3 Track and cant height

Contact wire height is defined as the distance between the contact wire and the track, measured perpendicular to the rail level. For a straight track, the rail level is horizontal, and the contact wire height coincides with the vertical distance. When the track geometry consists of curves, a cant height is introduced to compensate for centrifugal force. Since centrifugal force is a function of speed, the constructed cant height balances out forces for a given speed. Running vehicles at speeds higher or lower than this designated speed will result in some degree of tilting outwards or inwards, respectively, as shown in figure 2.10. Nowadays, many trains are equipped with a tilting mechanism, allowing for higher speed and more comfort for passengers when running through curves. A problem arises when tilting trains are run on a track designed for conventional trains; excessive lateral pantograph displacement. To overcome this problem, the pantographs must have some sort of active or passive displacement control, ensuring that no the contact wire stays within working range, as discussed in [17]. Table 2.2 shows the proportion of the major Norwegian railway tracks being curves. As much as 8 % has a curve radius less than 300 meters, which must be considered a sharp curve.

Table 2.2: Curves present on Norwegian railways [15]

Curve radius	Percentage
R $\leq$ 300 m	8 %
300 m $<$ R $\leq$ 500 m	15 %
500 m $<$ R $\leq$ 1100 m	15 %
R $>$ 1100 m	19 %
Straights	43 %

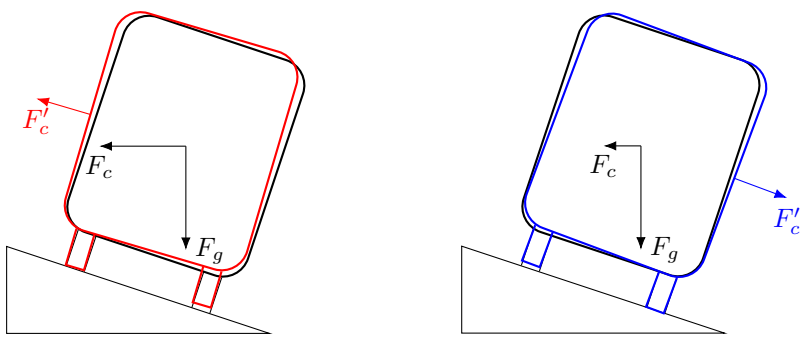

(a) High speed causing tilting outwards **(b)** Low speed causing tilting inwards

Figure 2.10: Centrifugal forces present in curves

2.3.1 Section lengths and overlaps

Some loss of tensile forces will occur along the wires, mostly due to curves, where force is diminished by the cantilevers. To keep the tension within an acceptable range, the overhead contact line is divided into several sections, where a midpoint anchor fixes the contact wire approximately halfway between the section ends. Kiessling *et al.* states that the total variation in tensile force should be less than 11 % [16], while BaneNor require documentation of a tensile force loss of less than 10 %. In Norway, the maximum tension length allowed is equal to 1500 meters [5]. Splitting the OCL into sections brings the need for overlaps. These can contain one to five spans, where the two overlapping sections run in parallel to ensure a smooth transition for the pantograph. For approximately one third of the middle overlapping span, the pantograph is in contact with both contact wires. This causes disturbance in the contact force, and thus it can be seen as an argument to utilise one-, three- or five-span overlaps, as this transition area will be mid span rather than at a support. A sketch outlining the overlap section for System 20 and System 25 can be found in appendix A

2.4 OCL Characteristics

2.4.1 Stagger

The contact line is constructed with a zigzag pattern, or *stagger*. By doing so, pantograph wear is significantly reduced, as the point of contact is shifted from side to side. However, too much displacement may result in the contact wire sliding off the collector strips, causing damage to the pantograph or OCL. According to BaneNor, the maximum stagger permitted for speeds of less than 160 km/h is 0.4 m, measured perpendicular to the track [5]. Stagger is maintained through the use of pull-off and push-off supports. In the case of curved track geometry, the stagger is kept at the outside, as the opposite would result in contact loss. This is illustrated in figure 2.12, while 2.11 shows the stagger for a straight track.

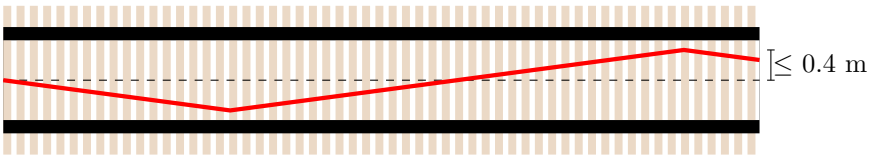

Figure 2.11: Stagger on a straight track, seen from above

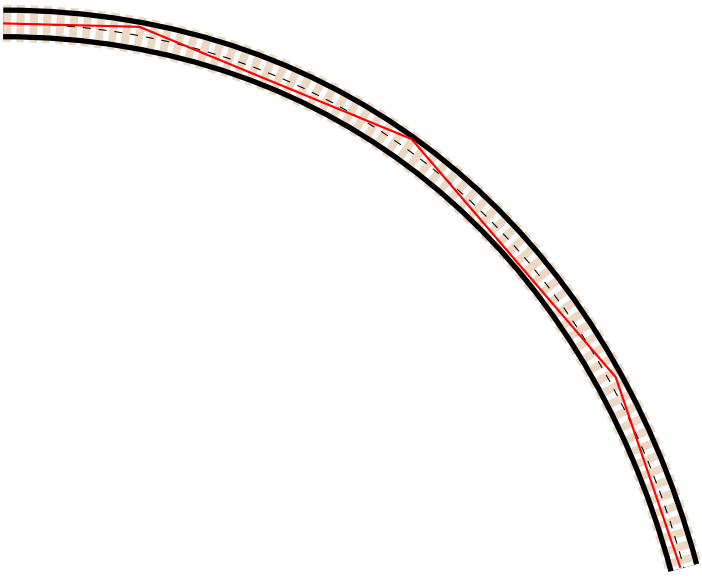

Figure 2.12: Stagger on a curved track, seen from above

2.4.2 Pre-sag

The vertical displacement of the contact line is denoted *sag*. For some system designs, the contact wire is provided with a pre-sag, meaning that the contact wire is lowered at the mid span relative to supports. When used correctly, such a pre-sag can help even out the effects of the changing elasticity over the span, and reduce the pantograph movement in vertical direction. At higher speeds, however, tests have shown that the application of pre-sag is unnecessary, and can even impair running characteristics [16]. For contact lines that are designed with pre-sag, a value between 0 and 0.05% of the span length is typical. As an example, a 60 m span with a pre-sag of 0.05% would lead to an initial vertical displacement of 3 cm. For high-speed railway lines, no variation in contact wire height is allowed, while the older system Table 54 is designed with a pre-sag of between 55 and 60 mm [14] .

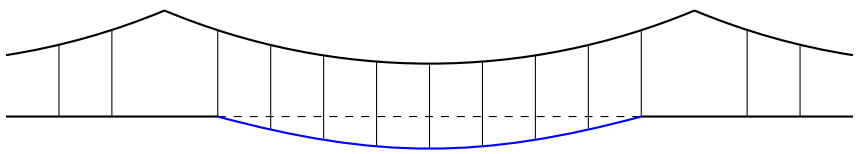

Figure 2.13: Pre-sag of a contact line

2.4.3 Elasticity

The *elasticity* of a contact line is a static quality. It describes the ratio between vertical displacement and vertical force along the span, and is therefore well presented through plots. Systems are designed with the purpose of keeping this elasticity as constant as possible throughout the span and section, allowing for higher speeds. The elasticity in the middle of a span can be approximated through the following equation:

$$e = \frac{L}{k \cdot (H_{CW} + H_{CA})} \tag{2.1}$$

where:

e = elasticity [mm/N]
L = span length [m]
H_{CW} = tension in contact wire [kN]
H_{CA} = tension in catenary wire [kN]
k = numerical factor

The numerical factor, k, equals 3.5 for contact lines with stitch wires, and 4.0 for lines without stitch wires.

Uniformity degree of elasticity is another static quality that is directly related to the elasticity. It describes the variation in elasticity, and is defined as:

$$u = 100 \cdot \frac{e_{max} - e_{min}}{e_{max} + e_{min}} \tag{2.2}$$

where the uniformity degree of elasticity, u, is a percentage, and e_{max} and e_{min} are the maximum and minimum elasticity in the given span. It is desirable to keep this value low, and at higher speeds it becomes critical.

Figure 2.14 shows the difference in elasticity for a stitched catenary design and

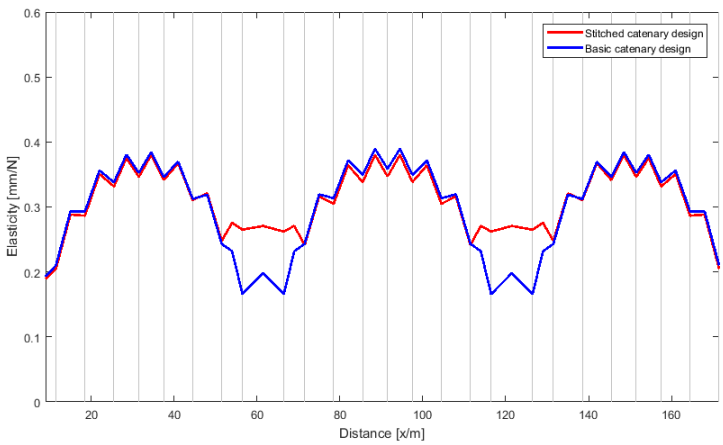

Figure 2.14: Elasticity plot for 3 spans (the plot is cropped to exclude the supports). Tension in CW and MW is 20 kN and 16 kN respectively. The stitch line tension is approximately 5 kN

a basic design. As can be seen, the maximum elasticity value is very similar for the two designs, but the stitched design clearly results in a more uniform elasticity, and thus better dynamic performance. The grey lines in the plot represents the dropper positions, and it is evident that they cause a slight drop in elasticity.

2.4.4 Tension

Both the catenary wire and the contact wire are stiffened by applying tension. Higher tension means additional stiffness, and thus the possibility for trains to operate at higher speeds. When TGV set the high-speed world record for conventional vehicles back in 2007 (574.8 km/h), the contact wire was tensioned at 40 kN. For comparison, System 20, which is a common OCS in Norway, utilises a tension of 10 kN.
The tensile force is applied to a tensioning section through a *tensioning mechanism*. These mechanisms are able to maintain the tension approximately constant despite changes in temperature. Both pulley and wheel tensioners depend on weights to achieve the desired tension, while hydraulic and electromechanical tensioning devices utilise gas and electricity respectively. Only the wheel and pulley tensioners (examples shown in figure 2.15), are in use for mainline railways [16].

(a) Pulley tensioning

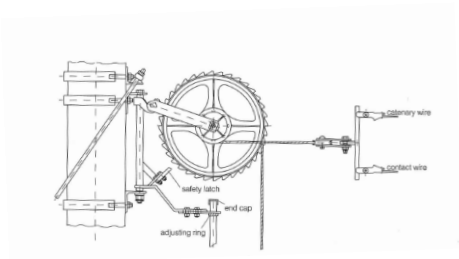

(b) Wheel tensioning [16]

Figure 2.15: Tensioning mechanisms

Chapter 3

Theory

3.1 Railway theory

3.1.1 Static force

The pantograph must exert a vertical force on the contact line in order for there to be any contact. For the static case, the resulting uplift depends only on the elasticity of the wire, and thus the relationship between the force and uplift can be described as:

$$y_{static} = F_0 \cdot e \tag{3.1}$$

where:

y_{static} = uplift at point of contact [mm]
F_0 = static force [N]
e = elasticity of the contact line [mm/N]

This also applies when low speed is considered,i.e. the interaction being quasi-static. As the speed increases, however, the dynamic effects become far more important.

3.1.2 Aerodynamic force

Aerodynamic uplift cause additional forces in the vertical direction. The magnitude of this force depends on running speed, pantograph design and weather conditions. In order for a pantograph to be approved, it must pass several tests in accordance with EN 50206-1. One of these tests, known as a *tethered test*, involves fixing the collector strips at a vertical position below the OCL, and performing test runs. The pantograph is equipped with a force measuring device, which then can be used for identification of the forces due to aerodynamic uplift. Pantograph manufacturers provide these as a function of speed. As an example, the aerodynamic force of Schunk's pantograph model WBL88 is found to be $0.0068v^2$ (speed given in m/s).

3.1.3 Dynamic force

To describe the behaviour of the contact line subjected to a vertical force at higher speed, the line is considered to behave like a flexible beam. The wire is assumed to have a specific mass, γ, and a longitudinal stress, σ. Due to transverse deflection, each element will experience a restoring force, F_y:

$$F_y = H_0 \cdot \sin(\alpha + d\alpha) - H_0 \cdot \sin(\alpha) \approx H_0 \cdot d\alpha \tag{3.2}$$

where H_0 is the longitudinal force.
With $\alpha \approx \tan(\alpha) = \frac{\partial y}{\partial x}$ and subsequently $d\alpha \approx dx \cdot \frac{\partial^2 y}{\partial x^2}$, the resulting restoring force is:

$$F_y = H_0 \cdot dx \cdot \frac{\partial^2 y}{\partial x^2} = \sigma \cdot A \cdot dx \cdot \frac{\partial^2 y}{\partial x^2} \tag{3.3}$$

The vertical force can be related to acceleration through Newton's second law:

$$F_a = m' \cdot dx \cdot \frac{\partial^2 y}{\partial t^2} = \gamma \cdot A \cdot dx \cdot \frac{\partial^2 y}{\partial t^2} \tag{3.4}$$

where m' is the mass of the wire element per length.

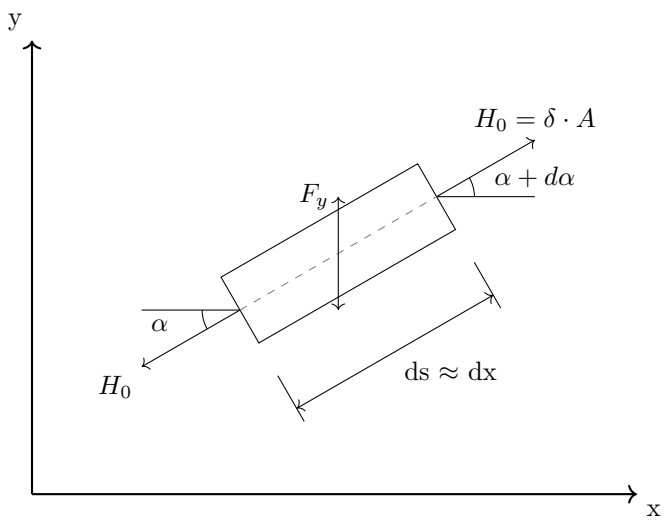

Figure 3.1: Forces acting on a CW element

Combination of equation 3.3 and 3.4 yields the equation known as the wave equation of a taut wire or string:

$$\frac{\partial^2 y}{\partial x^2} - \frac{\gamma}{\sigma}\frac{\partial^2 y}{\partial t^2} = 0 \tag{3.5}$$

The general solution to this equation is given by all functions of format:

$$y = f(x \pm c_p \cdot t) \tag{3.6}$$

where

$$c_p = \sqrt{\sigma/\gamma} = \sqrt{H_0/m'} \tag{3.7}$$

is the wave propagation speed. This property acts as a physical limit to energy transmission between contact wire and pantograph. This is shown by Kiessling *et al.* through introduction of the moving contact force to equation 3.5 [16]. The derivation is left out, but results in an uplift of:

$$y(x,t) = \frac{2F_0'l}{m'\pi^2(c_p^2 - v^2)} \cdot \sum_{n=1}^{\infty} \frac{1}{n^2} sin\frac{n\pi x}{l}(sin\frac{n\pi vt}{l} - \frac{v}{c_p} sin\frac{n\pi c_p t}{l} \tag{3.8}$$

The resonance characteristics of the wire can be observed from the first term, where a speed, v, closing towards the wave propagation speed will result in infinite uplift.

Dahlberg has investigated critical speeds for moving loads along a beam section, thus including bending stiffness [9]. He concludes that the first critical speed is:

$$c = c_{crit} = \sqrt{\frac{\pi^2 EI}{mL^2} + \frac{N}{m}} \tag{3.9}$$

where:

E = Youngs modulus [N/mm^2]
I = Moment of intertia [mm^4]
m = Mass per meter [kg/m]
L = Beam length [m]
N = Tensile force in beam [N]

The first term is often small compared to the second one, which leads to resemblance with equation 3.7, and a confirmation that the wave propagation speed acts as a physical boundary. A recommended maximum train speed of 0.7c to avoid deterioration of contact quality, was proposed by TSI [30], a value also referred to by others [3].

3.1.4 Reflection coefficient

The reason for the amplification of uplift when the speed increases is reflection of motion. When the waves travelling along the contact wire hit a point where movement is blocked, for example a dropper, a reaction force is exerted at the point, leading to a reflected wave. Kiessling *et al.* derives a reflection coefficient, r, for mass-free droppers:

$$r = -(y_r/y_0) = \frac{\sqrt{H_{CA}m'_{CA}}}{\sqrt{H_{CA}m'_{CA}} + \sqrt{H_{CW}m'_{CW}}} \tag{3.10}$$

where:

H_{CA} = Tensile force in catenary wire [N]
m'_{CA} = Mass per length in catenary wire [kg/m]
H_{CW} = Tensile force in contact wire [N]
m'_{CW} = Mass per length in contact wire [kg/m]

This reflection coefficient is part of the system characteristics, and can be reduced by reduction of catenary wire mass and tensile force in relation to the same parameters for the contact wire.

3.1.5 Doppler factor

Reflected waves by passive stationary masses are in general not amplified. However, when reflected waves meet up with waves from the travelling train, the total response can, depending on the OCL design, experience an amplification. The Doppler factor is defined as:

$$\alpha = (c_{CW} - v)/(c_{CW} + v) \tag{3.11}$$

where v is the speed of the train and c_{CW} is the wave propagation speed of the contact wire. When a train moves towards a discontinuity, a wave front will travel back and forth between the pantograph and the discontinuity until this point is reached. Whether this wave is amplified or damped depends on the ratio between the reflection coefficient and the Doppler factor; the *amplification coefficient*, γ_A.

$$\gamma_A = \frac{r}{\alpha} \tag{3.12}$$

A γ_A-value > 1 results in amplification rather than damping. Many considerations must be made when designing OCL systems, and despite the drawback of more energy in the system, many standard systems are delivered with an amplification coefficient of well above 1. For example, the Re250 system comes with an amplification factor of 1.63.

Table 3.1 shows the dynamic characteristics of systems used in Norway. The values used for Table 54 corresponds to the "new" configuration, whereas a combination of contact wire tension of 625 kg and catenary wire tension of 500 kg was used earlier.

Table 3.1: Overhead Contact Line Systems currently installed in Norway

System	H_{CW} [N]	H_{CA} [N]	c_p [km/h]	r
System 25	15000	15000	427	0.43
System 20	10000	10000	382	0.42
System 35	7060	7060	321	0.42
Table 54	10000	5000	382	0.33

3.2 Dynamics

3.2.1 Finite elements

The Finite Element Method (FEM) is used for modelling of both catenary and pantograph in ABAQUS. Full explanation of the concept is presented by Cook in [8]. In short, all nodal positions and their relative connections are stored in matrices;

$$[\mathbf{M}]\{\ddot{\mathbf{D}}\} + [\mathbf{C}]\{\dot{\mathbf{D}}\} + [\mathbf{K}]\{\mathbf{D}\} = \{\mathbf{R^{ext}}\} \tag{3.13}$$

where $\mathbf{M}$ is the global mass matrix, $\mathbf{C}$ is the global damping matrix, $\mathbf{K}$ is the global stiffness matrix and $\mathbf{R^{ext}}$ is a matrix containing external forces. The size of these matrices depends on the model size, and all the dynamic equations must be satisfied at all time.

3.2.2 Damping

A catenary system is considered to be a lightly damped structure. This means that the wires continue to vibrate for a long time after a pantograph has passed. The damping is difficult to measure and model, but is generally thought to be in the order of 1 % of critical damping [20].
A common way to introduce damping to the system, is the use of mass and stiffness proportional damping, also called Rayleigh damping. The damping matrix is then constructed as a linear combination of the mass and stiffness matrix:

$$[\mathbf{C}] = \alpha[\mathbf{M}] + \beta[\mathbf{K}] \tag{3.14}$$

where α and β are damping coefficients. The damping ratio can be found from these coefficients, as depicted in figure 3.2. For lower frequencies, the mass contribution dominates relative to the stiffness. In [18], Nåvik identifies damping coefficients for catenary systems through full-scale measurements and covariance-driven stotchastic subspace identification (Cov-SSI). The resulting values, $\alpha = 0.062$ and $\beta = 6.13\text{e}{-06}$, are adopted in this thesis.

3.2.3 Numerical integration

Both *explicit* and *implicit* integration methods are available in the ABAQUS environment; Explicit and Standard respectively. The methods have their pros and cons, such as the explicit being faster but conditionally stable, whereas an implicit dynamic analysis is heavier, but unconditionally stable, allowing for larger time increments. An implicit method, namely the (α-method) proposed by Hilber-Hughes-Taylor, is chosen for simulation [13]. This is a generalisation of the Newmark methods, and is based on the Newmark relations:

$$\{\dot{\mathbf{D}}\}_{n+1} = \{\dot{\mathbf{D}}\}_n + \Delta t\left[\gamma\{\ddot{\mathbf{D}}\}_{n+1} + (1-\gamma)\{\ddot{\mathbf{D}}\}_n\right] \tag{3.15a}$$

$$\{\mathbf{D}\}_{n+1} = \{\mathbf{D}\}_n + \Delta t\{\dot{\mathbf{D}}\}_n + \frac{1}{2}\Delta t^2\left[2\beta\{\ddot{\mathbf{D}}\}_{n+1} + (1-2\beta)\{\ddot{\mathbf{D}}\}_n\right] \tag{3.15b}$$

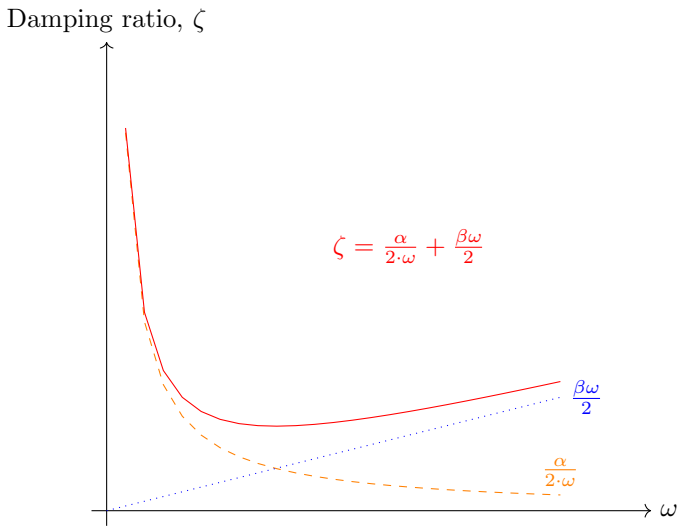

Figure 3.2: Proportional damping

where γ and β are numerical factors controlling characteristics such as accuracy and numerical stability. The modified equation of motion becomes:

$$\begin{aligned}[\mathbf{M}]\{\ddot{\mathbf{D}}\}_{n+1} + (1+\alpha)[\mathbf{C}]\{\dot{\mathbf{D}}\}_{n+1} - \alpha[\mathbf{C}]\{\dot{\mathbf{D}}\}_n \\ + (1+\alpha)[\mathbf{K}]\{\mathbf{D}\}_{n+1} - \alpha[\mathbf{K}]\{\mathbf{D}\}_n = \{\mathbf{R}_\alpha^{\mathbf{ext}}\}\end{aligned} \tag{3.16}$$

where α controls the amount of algorithmic damping, and $\mathbf{R}_\alpha^{ext}$ is $\mathbf{R}^{ext}$ evaluated at time $(t_{n+1} + \alpha\Delta t)$. While the Newmark methods fail to retain second-order accuracy when introducing algorithmic damping, this can be maintained with the α-method. A value of $-\frac{1}{3} \leq \alpha \leq 0$ is recommended [8], and ABAQUS applies the default value of $\alpha = -0.05$ in order to remove high-frequency noise without affecting the lower frequency response significantly [29].

3.3 Natural Frequencies

All structures with mass and stiffness tend to vibrate freely at one or several frequencies, depending on the degree of freedom. These frequencies are called natural frequencies or eigenfrequencies. The complexity of the overhead contact line leads to a multitude of natural frequencies. Identification of the frequencies in a real system can be done by performing impact tests with suitable equipment, such as an instrumented hammer. In FEA environment, natural frequencies are identified through equation solving. The eigenvalue problem for natural frequencies of an undamped FE model is given as

$$(-\omega^2 M^{MN} + K^{KM})\phi^N = 0 \tag{3.17}$$

where

M^{MN} = Mass matrix
K^{MN} = Stiffness matrix
ω = Frequency
ϕ^N = Eigenvector, also called mode of vibration
M, N = Degrees of freedom

When the natural frequencies and the corresponding eigenvectors are identified, the *generalised mass*, m_α can be calculated as

$$m_\alpha = \phi_\alpha^N M^{NM} \phi_\alpha^M \tag{3.18}$$

Notice that this generalised mass is a scalar quantity. Furthermore, a modal *participation factor*, $\Gamma_{\alpha i}$ is defined as:

$$\Gamma_{\alpha i} = \frac{1}{m_\alpha} \phi_\alpha^N M^{NM} T_i^M \tag{3.19}$$

where T_i^M is a matrix defining the magnitude of the rigid body response of degree of freedom M, to a rigid body motion of type i [26]. Here, i represents the six possible rigid body motions directions; the global x-,y- and z-direction, and the rotations about these axis. The participation factor thus indicates how strongly a motion in direction i is represented in the relevant eigenvector.
The *modal effective mass* is defined as

$$m_{\alpha i}^{eff} = (\Gamma_{\alpha i})^2 m_{\alpha i} \tag{3.20}$$

where α is the mode and i is the associated direction. Summation of modal effective mass for each of the 6 directions should yield the total mass of the model. This may serve as a tool for identifying how many modes that should be considered in a modal analysis. A summed effective mass that is not close to the total mass, suggests that more modes should be included in the analysis. The effective modal mass also helps identifying the most important frequencies, where large parts of the model will be excited.

3.4 Filtering

EN 50318, *Validation of simulation of the dynamic interaction between pantograph and overhead contact line*, states that the frequency range of interest is from 0 to 20 Hz. The sampling frequency should be well above 20 Hz (equivalent to a time step of 0.05 s) to represent a realistic model, and thus filtering of output is required. Type of filter is not specified in the standards. All filtering in this thesis is handled by MATLAB, which provides several filtering options. Both a Butterworth filter and a Chebyshev filter have been tested. The latter enables a steeper roll-off, but introduces an unwanted passband ripple, as illustrated in figure 3.3. The magnitude of this ripple can be set to a low value, but this reduces the roll-off steepness. Since steepness can also be acquired through the order of the filter, a Butterworth filter of higher order is chosen. EN 50318 does not specify the order of the filter to be used, however, EN 50317, *Requirements for and validation of measurements of the dynamic interaction between pantograph and overhead contact line*, requires low-pass filters to be of sixth order or higher.

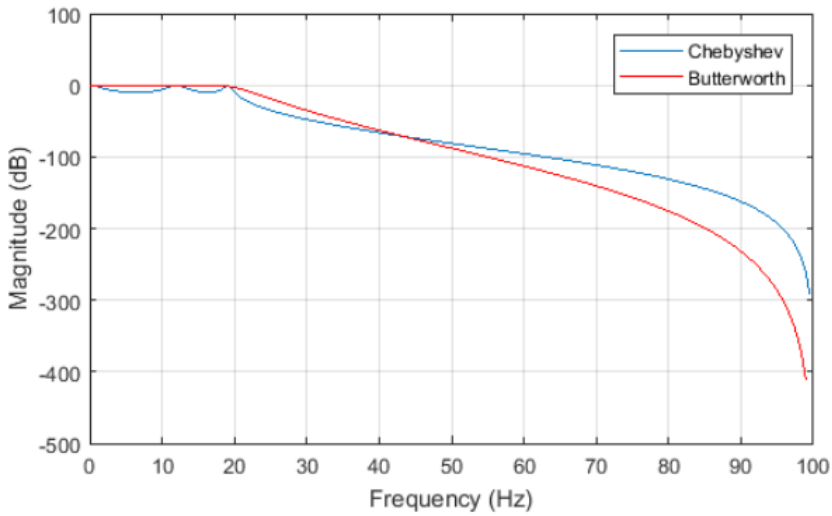

Figure 3.3: Butterworth filter compared to a Chebyshev filter, both with a cutoff frequency of 20 Hz

Chapter 4

Numerical modelling

4.1 General

The interaction between catenary system and pantograph can be modelled in several different ways. One alternative is to build the static catenary system with finite elements, and to represent the pantograph through a multibody description, as depicted in figure 4.1a[4]. The two systems are then co-simulated by applying a contact module. In [24] the catenary is modelled based on Absolute Nodal Coordinate Formulation (ANCF) to ensure inclusion of nonlinear effects. Another alternative is to model the pantograph solely in FEA software, as has been done by Qian *et al.* in [21]. A pantograph constructed with finite elements improves the resemblance to a real-world pantograph, however at the price of computational power. Many aspects of the catenary/pantograph interaction can also be examined through the use of a simple lumped-mass model. In this thesis, the catenary is modelled with beam elements, and the pantograph is a lumped-mass model where the collector strips are included as beams.

The model proposed in this thesis has been created to run in the Finite Element Analysis (FEA) software ABAQUS. This software provides a well developed graphical user interface, the *Complete Abaqus Environment* (CAE), which can be used for modelling. A catenary-pantograph model is complex, and some functionality, such as the edge to edge contact formulation, is not yet available in CAE. This encourages the use of *python scripts*, an approach that also provides more control. The Abaqus Scripting Reference Guide [28] lists several methods and functions for direct use with the Abaqus environment. Thus, a model can be created based on such commands. Another approach, and the one that has been used in this thesis, is the use of *input files*. An input file is basically a text file with model data, sorted under certain keywords. When ABAQUS runs an input file, these keywords are interpreted sequentially, and a model is built. The ABAQUS Keywords Reference Guide [27] lists all the available keywords and respective inputs.
Input files (.inp) are also generated for cases where the model initially was built in

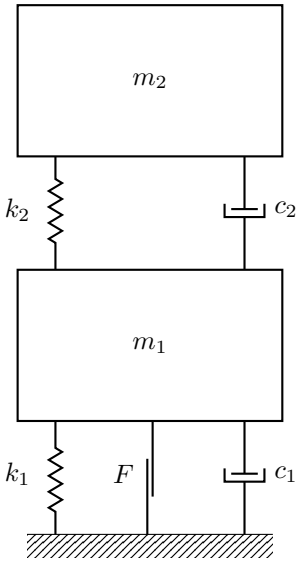

(a) Lumped-mass model

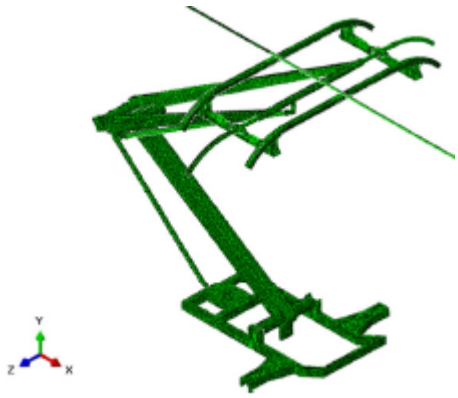

(b) Complete pantograph model built in FEM software [21]

Figure 4.1: Two different pantograph models

CAE. It can therefore be useful to model parts in the graphical user interface, and examine the input files afterwards. This is a technique that also can be utilised when working with python scripts, since script files are generated as .jnl-files in the working directory.

4.2 Python

Python is a high-level programming language created back in 1991. One of its perks is the readability resulting from wide use of spaces and indentation. Python supports object-oriented programming; a concept well suited for writing numerical model code. The idea is to define certain objects, and equip these with variables and methods/functions only accessible to the object itself. As an example, a catenary system can be made as an object, and then told to add a span from point A to B, with given properties. An object-oriented approach is adapted in the attached python code, however, as the author is by no means an expert programmer, proficient coders would probably frown upon certain aspects of it. Comments are widely used throughout the scripts to explain the different features. If the reader is completely unfamiliar with the coding language, a quick look at one of the many python programming guides online may be useful.

4.3 The numerical model

A few early attempts at modelling directly through python scripts were made, but it appeared to be more cumbersome, and the input file approach was given priority. All input files are written with the aid of python, which provides excellent control over crucial parameters, such as span lengths, element lengths, temperature fields, etc. The sequential structure of a python script, in addition to loop functionality, makes it well suited for parametric studies.
General information about the model is presented in the subsequent sections.

4.3.1 Objective

Drugge *et al.* presents an overview of prerequisites for model creation in [10]. Here, both model features and aspects such as usability and efficiency are included. Some of the most important points are repeated in the list below:

- Consistent method for set up of simulation models
- Techniques to set up models of combinations of substructures
- Type of catenary system
- Number of sections
- Number of spans
- Velocity of train
- Span lengths, system height, stagger, wire height, dropper positions
- Type of supporting structure
- Curve radius and direction, superelevation of tracks
- Mass and inertia properties for pantographs
- Characteristics for springs, dampers, bump stops etc.
- Static and aerodynamic forces
- Model detail
- Visualisation possibilities, post-processing, user-friendly

The objective when creating the model code, was to fulfil as many of these requirements as possible. Code efficiency has not been given priority in this thesis.

4.3.2 Beams

All wires in the numerical model are made as beams. This is a common approach when the catenary system is modelled in FEM software, and introduces bending stiffness to the wires. Poetch [20] concludes that the differences between an Euler-Bernoulli beam model and a Timoshenko beam model are small, and that it should be sufficient to use Euler-Bernoulli beams (B33 in Abaqus). However, modelling with such elements led to convergence difficulties, and therefore Timoshenko beam elements (B32) were chosen. In [2], Rønnquist and Nåvik also utilise Timoshenko beams in order to maintain numerical stability. It should be emphasised that the reason for choosing these elements is not the inclusion of shear deformation and rotatory inertia.
An attempt to include stitch wires in the model was made, however, due to time limitation, the full implementation was not completed. The stitch wire design is functional for straight track segments, but achieving the correct tension remains a problem, and must be done through manual iteration.
Though the catenary wire is a stranded wire, it is assigned a circular profile in the model. This means a small increase in area compared to a real wire, but is considered not to have a large impact on the results.

4.3.3 Droppers

In order for the model to be realistic, it should include the possibility for dropper slackening. This highly non-linear event occurs when the contact wire is lifted, and the proximate droppers enter a state of compression rather than tension. In this state, the dropper wires have no resistance to motion. Where some authors choose to circumvent the problem, and model the droppers as linear [31], a variety of approaches to include the non-linearity exist in the literature. Some proposed methods are the application of concentrated nodal forces [1], contact wire connected to the catenary wire by means of spring-mass-dampers [12], and the use of non-linear truss elements where the global stiffness matrix is updated continuously [25].

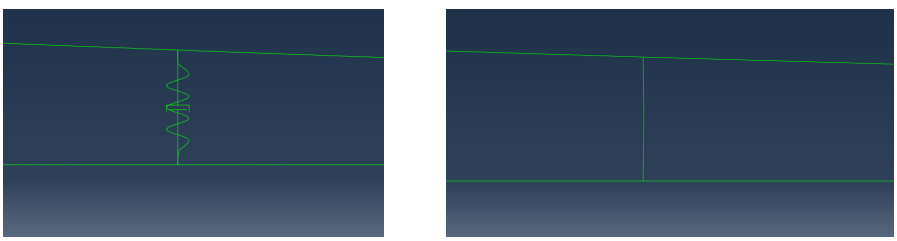

(a) (b)

Figure 4.2: (a) Spring-damper dropper. (b) Beam dropper. A slight deflection is observed

The model developed in thesis thesis includes the possibility to model the droppers as nonlinear spring-dampers or as beam elements. Figure 4.2 shows the difference between the two approaches. In the case of beam element droppers, the

beams are given an initial deflection in order for lateral bending to occur when compressed, a strategy also utilised by Nåvik in [19]. The spring elements can be defined as nonlinear springs in ABAQUS. Figure 4.3 confirms that the elements are unable to withstand any compression.

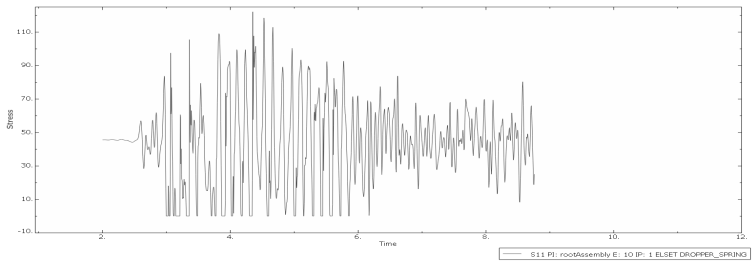

Figure 4.3: Time series of stress in a dropper spring

The developed code includes several ways of specifying the dropper positions. One distinction is whether the dropper height is provided or not. If it is, the catenary wire coordinates are placed accordingly to these heights along the span. The coordinates between the dropper points are found through linear interpolation. Dropper positions can also be given as either an integer or a list of positions along the span. This will return a catenary wire approximated as a parabola, where the height at the mid span is a system parameter found through iterations. Being able to find the appropriate dropper heights automatically for a designated pre-sag, would have improved the code. Figure shows two spans of 60 meters where the droppers are provided as '5' and '[3,13,23,37,47,57]', respectively.
The droppers are not assigned any mass, but a mass element representing both the dropper and the dropper clip is placed at every connection point.

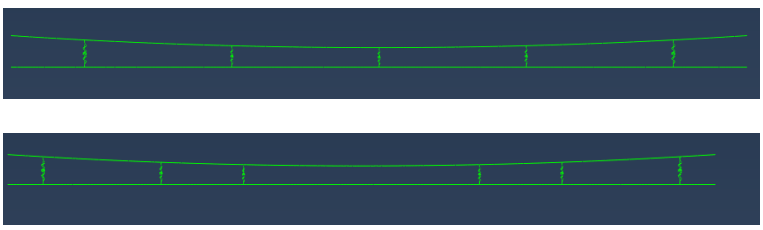

Figure 4.4: Droppers specified in two different ways

4.3.4 Brackets

Modelling of the bracket itself has been omitted in the model. At each support, the catenary wire is pinned, whereas the contact wire is restricted in the horizontal direction perpendicular to the wire. It is important to apply this latter boundary condition in relation to a local coordinate system. Using the global coordinate system results in erroneous boundaries when the geometry is three-dimensional. In order to cope with singularity errors that were encountered with the given boundary conditions, one rotational degree of freedom was also constrained, namely UR1.

4.3.5 Track geometry

The track geometry is used as a reference for the catenary system, and is also included in the model as a display part. Including it as a display part helps identifying errors in track geometry without affecting the model size particularly. Placement of supports is handled by an algorithm that loops through the track geometry, ensuring that all coordinates are in accordance with given conditions, such as stagger and span length.
Since only the centre line of the track is modelled, cant height is incorporated by elevating the track by 50% of the original cant height, and applying a rotation to the train reference point. Figure 4.5 shows how this rotation changes as the train passes from one curve to another. Parts of the graph where the angle increases or decreases corresponds to a *clothoid*, or a transition curve, in the track geometry.

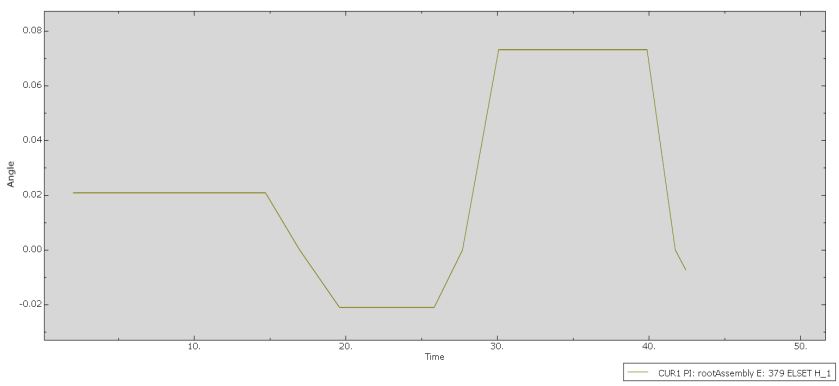

Figure 4.5: Train rotation along a section containing curves in both directions

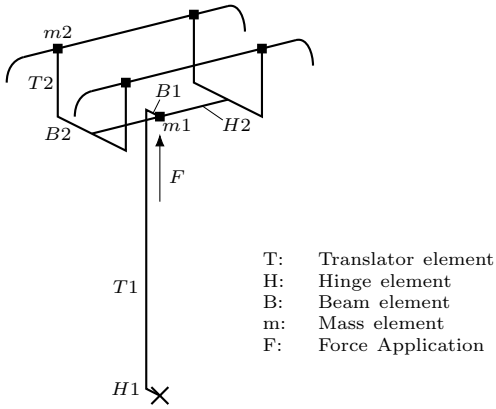

Figure 4.6: Pantograph as modelled in ABAQUS (not in scale)

4.3.6 Pantograph

The pantograph is modelled by assembling several connector elements, and attaching these to the collector head, as depicted in figure 4.6. The ABAQUS connection-type library contains multiple connectors that serve the purpose to constrain nodes in relation to each other. The library ranges from simple connectors joining two nodal positions, to elements modelling material flow between two nodes. Elements used in the pantograph model are of the type *translator*, *beam* and *hinge*. Beam elements provide a rigid connection between two nodes, constraining all 6 DOF. In translators and hinges, one of these are released, U1 and UR1 respectively, thus enabling relative motion between nodes. The connector behaviour, including for example elasticity, damping and friction can also be specified.
The collector head is modelled as two beams with the design specified in EN 50367, and shown in figure 4.7. By doing so, an edge-to-edge formulation can be used when defining contact interaction.

A somewhat modified lumped-mass model of Schunk's pantograph WBL85 has been used for most simulations. The parameters for this model, are given in table 4.1.

Model	WBL 85
m1[kg]	16.5
k1[N/m]	100
c1[Ns/m]	63.5
m2[kg]	4.6/4
k2[N/m]	6200/4
c2[Ns/m]	20/4
F [N]	55

Table 4.1: Pantograph parameters

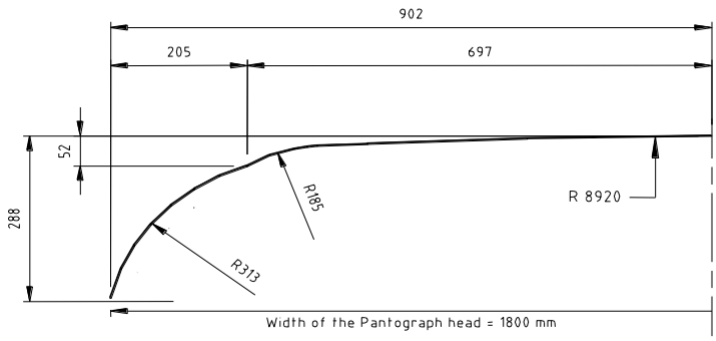

Figure 4.7: Pantograph head dimensions according to EN 50367, Figure B.5

4.4 Steps

Analysis is performed by running several steps. Different steps can be included or suppressed depending on analysis type. The available steps in the proposed model are:

- **Tension and gravity**: A static step that introduces both tension and gravity to the catenary wire and contact wire. At early stages, tension and gravity were introduced in separate steps. This approach resulted in singularity issues. Merging the two steps significantly reduced the frequency of these errors. Nåvik confirms the importance of adding these forces simultaneously in [19].

- **Pantograph force**: A static step that applies both the static and aerodynamic force to the pantograph, which in turn establish contact between the pantograph and the contact wire.

- **Elasticity**: A static step for identification of the elasticity along the span. In this step, a force of 100 N is applied to several nodes in the contact wire, one point at a time, and the resulting uplift is stored in a .dat-file. Data can be extracted from this file using for example a MATLAB script, and plotted for visualisation.

- **Modal analysis**: This step can be included to investigate the system's eigenfrequencies. It is in reality two steps; first a step extracting eigenfrequencies for the undamped system, and secondly a complex eigenvalue extraction. The latter is able to include effects such as damping and friction.

- **Movement**: A dynamic step for movement of the pantograph. Motion is achieved through the use of prescribed displacements. Before the step is run, a python function evaluates the track geometry and train speed, and generates an input file containing all relevant displacements at given time steps. This

file is then included through the use of the keyword *INCLUDE. The usage of boundary conditions for prescribing translations is quite straight forward. Rotation, on the other hand, introduces a few more considerations. This is explained in 4.6.2.

4.5 Contact

When dealing with catenary/pantograph interaction, the contact definition is crucial. ABAQUS offers multiple approaches for contact inclusion. In ABAQUS/Standard the options are:

- General contact
- Contact Pairs
- Contact elements

The approaches are based on complex contact algorithms, and share a large proportion of the framework. Parts of the algorithms are, however, unique, which leads to advantages and limitations for each of them. The differences between these will not be discussed any further in this thesis, but can be found in the user guide [26]. A general contact approach has been used in the model, more specifically an edge-to-edge formulation. This type of formulation is developed to be more efficient when the contact occurs between two edges, such as beams. The edge-to-edge option is not yet available in ABAQUS CAE, and must therefore be used in combination with input files. At early stages, a contact description based on contact pairs and master/slave surface was attempted. Compared to the edge-to-edge formulation, this approach demanded the use of smaller elements, and also appeared less reliable.
When modelling contact forces, ABAQUS requires the specification of surface interaction. In the model, a hard contact relationship, which is also the default, is used. This option minimises the surface penetration, and is strict compared to softened contact. The difference between these two contact pressure-overclosure relationships are shown in figure 4.8. Contact constraint is enforced through the linear penalty method, a method where the contact force is made proportional to the penetration distance. Analogue to any spring, the constant relating the two variables is called penalty stiffness, by default set to 10 times a representative underlying element stiffness. It can also be set manually by user. Though ABAQUS allows for both a direct method and the augmented Lagrange method(based on a penalty method), penalty methods are often preferred, as they provide some numerical softening in addition to efficiency.

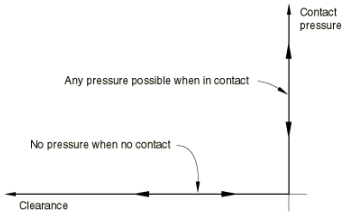

(a) Hard pressure-overclosure relationship

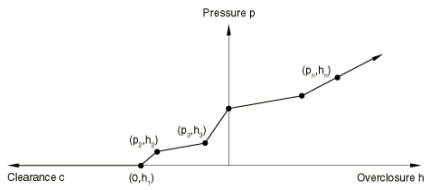

(b) Soft pressure-overclosure relationship, based on tabular input

Figure 4.8: Contact relationships [26]

4.6 Challenges

4.6.1 Applying tension to wires

Application of tension to the OCL proves to be a challenge in ABAQUS. Though it is probably a possibility to model a full tensioning system with for example pulleys, this is a cumbersome task. Another approach is the use of bolt load. This feature is originally meant to be used for modelling of bolts, and provides the option to include tightening forces or length adjustments in these. However, bolt loads can also be used to apply forces to a beam, the main advantage being the direct application of tension force value. A partition of the beam cross-section in addition to a node used for force application, must be defined for each tensioning span. This approach was given several attempts, but in the end proved to be a demanding task.

The method used in the model is based on temperature. Thermal expansion is the tendency of materials to expand or shrink when subjected to temperature change. The relationship is given as

$$\epsilon_T = \alpha_T \cdot \Delta T \tag{4.1}$$

where ϵ_T is the thermal strain, α_T is the material specific thermal expansion coefficient, and ΔT is the change in temperature. By fixing the beam end points and lowering the temperature, the beams are thus subjected to a tension force. However, identification of the temperature that corresponds to the desired tension, is not a straight forward process. The OCL is a complex system, where contact wire and catenary wire is connected through the droppers. Thus, changing the tension in one wire affects the other. Displacement of the contact wire in vertical direction is also important to consider, as too much sag is unacceptable. This sag is a function of tension in contact wire and catenary wire, span length and dropper lengths.

To get an overview of how the outcome is influenced by these parameters, a variance-based sensitivity analysis was performed. It should be emphasised that this was only to get a basic understanding of how the parameters were related, and not in any means a thorough analysis. The method used to obtain the results is outlined by Saltelli *et al.* in [23]. Due to possible errors in implementation and far too few simulation rounds, these results function only as a guideline. The output's

dependency on the four parameters is shown in table 4.2, while figure 4.9 provides some visual aid. A small value implies little dependency, whereas a large value corresponds to high dependency. The parameter "Ratio" is the ratio of the dropper length at mid span to the system height, the catenary wire being modelled as a parabola.

Table 4.2: Variable dependency of outputs [%]

Output variable	Span Length	Ratio	CW Temp.	MW Temp.
Sag	63.7	30.6	1.2	4.5
Tension CW	0.4	0.3	99.2	0.1
Tension MW	17.1	6.1	0.3	76.5

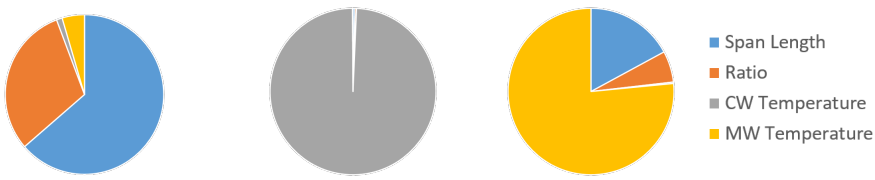

(a) Sag **(b)** CW tension **(c)** MW tension

Figure 4.9: Output sensitivity

Expressing each of these outputs as functions of the four inputs would simplify the process of finding the right combinations. This is unfortunately not an easy task, and therefore a more primitive method is used. Acceptable configurations are found through several simulations where the input parameters are altered. In this process, the sensitivity analysis proves a tool, providing information of what movements can be expected when adjusting certain input values.
In *Contact Lines for Electric Railways* Kiessling *et al.* derives an expression for the catenary wire height

$$y_{CA} = \frac{G'_{OCL}}{H_{CA}} \cdot \frac{x^2}{2} + y_{OCL} \tag{4.2}$$

where

G'_{OCL} = weight of the OCL per meter [N/m]
H_{CA} = catenary wire tension [N]
y_{OCL} = catenary wire height at mid span [m]
x = distance from mid span [m]

Unfortunately, dropper adjustment according to this equation was less successful. More strict control over the tension and displacement would undoubtedly have been favourable.

4.6.2 Modelling of cant height

The addition of translations is a *commutative* operation, i.e., the order in which the translations are added, does not affect the resulting displacement. This can easily be illustrated by adding vectors in different order, as shown in figure 4.10. On the other hand, the addition of rotation is a non-commutative operation, i.e.,

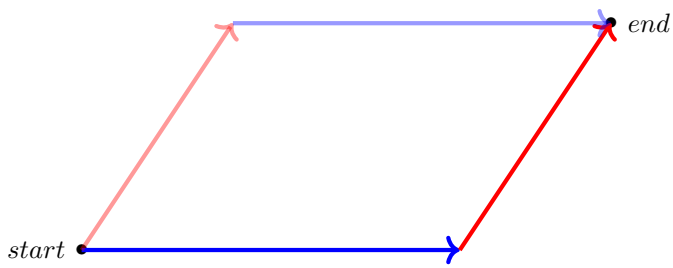

Figure 4.10: Vector addition in 2D

the final displacement *does* depend on the order in which the rotations were added. This can be illustrated by considering a coloured cube, as depicted in figure 4.11. It is obvious that the final orientation of the cube depends on the rotation order.

The fact that addition of rotation is non-commutative, presents a challenge when

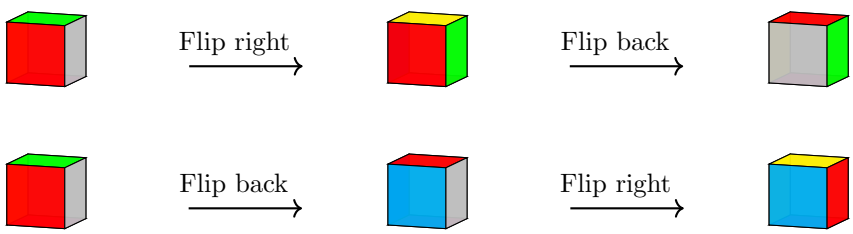

Figure 4.11: Rotation of cube in two different orders

track curves *and* a rotation about track axis is included in the ABAQUS model. When boundaries are prescribed in ABAQUS, they are given relative to a globally or locally defined coordinate system. In dynamic analysis, it would be favourable to describe rotations relative to a moving coordinate system, i.e. *intrinsic* rotations. However, ABAQUS Analysis User Guide informs regarding transformed coordinate systems that "*These transformed directions are fixed in space; the directions do not rotate as the node moves.*"[26]. As the functionality is already implemented in connector elements, it is not unlikely that such a feature does indeed exist, however a workaround has been proposed in this thesis.

Track angle is included in the model through the use of a connector element, specifically a hinge. This hinge is attached at the bottom of the pantograph. Hinge elements allow for behaviour such as spring stiffness to be specified. Since

$$M = k_\phi \cdot \phi -> \phi = \frac{M}{k_\phi} \tag{4.3}$$

where M is a moment, k_ϕ the spring constant and ϕ the angle, this angle can be controlled by the applied moment. Concentrated forces and moments can be specified with the option "FOLLOWER", instructing the force to follow the nodal rotation. In order to prevent the pantograph/catenary interaction from having an effect on the track angle, both spring stiffness and the moment are set to values of large magnitude.

Chapter 5

Results and Discussion

5.1 Constructing the model code

A large proportion of the overall work related to this thesis has been put into code development. The aim was to create a versatile code, where parameters could be altered with ease, making it possible to examine several phenomenons with little effort. Many of the prerequisites outlined in 4.3.1 have been successfully implemented, while a combination of time limitation and prioritising lead to others being abandoned.

5.2 Tension and displacement control

The aim of this short section is to show how important initial geometry is for contact parameters. A portion of a real catenary section, located in Soknedal as part of Dovrebanen, is simulated with droppers positioned as tabulated in appendix A, and droppers placed in a way that reduces the sag. The speed is set to 110 km/h. Figure 5.1 shows the contact wire height for the two different cases, and the initial geometry (no cant height was included in this model, thus contact wire height coincides with the vertical height). The geometry with less sag is far more uniform, but it can be seen that the whole contact line is lowered, also at the supports, which is not optimal. For the geometry with more sag, large displacements can be observed at the beginning and end of the total catenary. This is due to erroneous dropper configurations, as the outer droppers were designed for a different system height. Since the shaded areas are excluded from the analysis, this will not affect the results.

Contact force and pantograph movement for the designated section is illustrated in figure 5.2. Whereas the contact forces have same mean value, 61.6 kN, the force for geometry with more sag fluctuates more. The two resulting standard deviations are 7.7 kN and 5.8 kN. In figure 5.2b the pantograph movement is seen to be opposite for the two geometries. For the model with more sag, this sag pushes the pantograph down, forcing it to move along with the track geometry. In the other

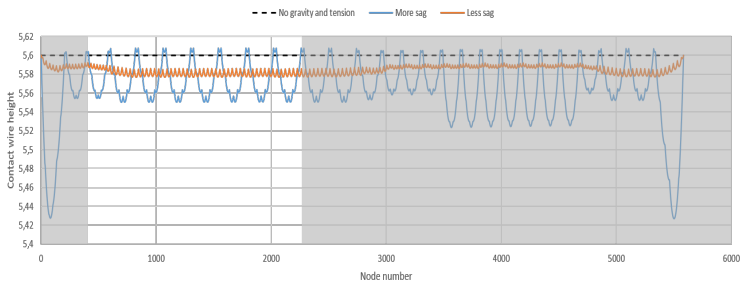

Figure 5.1: Contact wire displacement in vertical direction

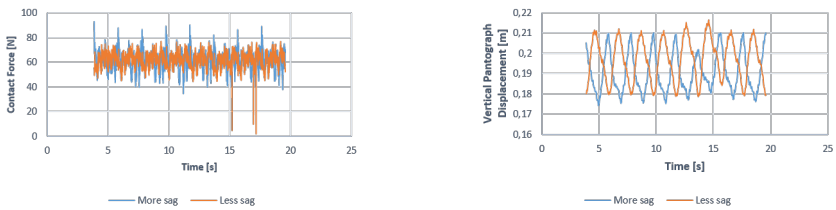

(a) Contact Force **(b)** Vertical pantograph displacement

Figure 5.2

case, too little sag to counteract the elasticity is included, and the pantograph reaches its peak at the mid span. Both the pantograph movement and contact fore time series suggests that difference in pre-sag reduces the comparability for other parameters. Strict control over tension and displacement is strongly advised.

5.3 Performance parameters

When performing catenary/pantograph interaction simulations, the contact force is considered to be the most important parameter to extract. In EN 50318 contact force is defined as "*vertical force applied by the pantograph to the overhead contact line. The contact force is the sum of the forces of all components*"[11]. Time series of this force tells whether contact is maintained or lost, and also shows the deviations over the section. The mean contact force, F_M, and the standard deviation, σ, are indicators used for performance assessment. A low standard deviation implies small dynamic contact force fluctuations and good dynamic performance of the system, while the opposite indicates poorer dynamic performance. The minimum and maximum values of contact force are also of interest. A minimum value of zero indicates contact loss whilst a large maximum value can cause damage to the system. The uplift at supports is also measured, since a large value may cause the steady arm to hit the registration arm.

5.4 Validation

To gain some confidence in the model, it is tested according to the validation procedures outlined in EN 50318. This standard describes a scenario for simulation, along with certain expected output values.These values have been found through several verified simulations. Briefly explained, the track to be simulated is a high-speed line over 10 straight spans, each of 60 meters with specified dropper positions and stagger. Such a span is shown in figure 5.3.

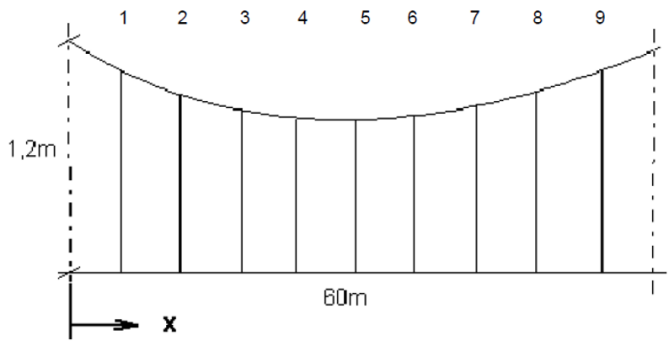

span length = 60 m
encumbrance = 1,2 m
stagger = ± 0,2 m

Dropper	1	2	3	4	5	6	7	8	9
X [m]	5	10,5	17,0	23,5	30,0	36,5	43,0	49,5	55,0

Figure 5.3: Span to be used for validation, according to EN 50318 [11]

Specific weight, dropper stiffness, registration arm modelling and encumbrance is also specified. A lumped-mass pantograph model is provided along with relevant input values. Simulations are supposed to be performed in two rounds, with speeds of 250 km/h and 300 km/h, and the contact forces and vertical displacements are recorded for span 5 and 6. The frequency range of interest is set to 0-20 Hz. Table 5.1 renders the ranges which simulation results should be within.

Table 5.1: Range of results from reference model

Speed [km/h]	250	300
F_M [N]	110 to 120	110 to 120
σ [N]	26 to 31	32 to 40
Statistical maximum of contact force [N]	190 to 210	210 to 230
Statistical minimum of contact force [N]	20 to 40	-5 to 20
Actual maximum of contact force [N]	175 to 210	190 to 225
Actual minimum of contact force [N]	50 to 75	30 to 55
Maximum uplift at support [mm]	48 to 55	55 to 65
Percentage of loss of contact [%]	0	0

Both a model made up with beam element droppers and one with spring-damper droppers have been tested. For each of these approaches, models are built up with element lengths of 0.25 meters and 0.5 meters. The results are filtered with a 6th order Butterworth low-pass filter with a cut-off frequency of 20 Hz. The results are presented in table 5.2 and 5.3. Here, the model names are abbreviated so that 'beam25' refers to a model with beam droppers and element lengths of 0.25 meters.

As can be seen, neither of the models pass the validation test, and should in

Table 5.2: Validation 250 km/h

	250 km/h							
	beam25		beam50		spr25		spr50	
F_M [N]	118.4	✓	118.3	✓	117.8	✓	117.8	✓
σ [N]	37.0	x	36.9	x	27.7	✓	27.7	✓
Stat. max. [N]	229.4	x	229.0	x	200.8	✓	200.9	✓
Stat. min. [N]	7.4	x	7.6	x	34.7	✓	34.7	✓
Actual max. [N]	233.6	x	233.4	x	185.2	✓	185.1	✓
Actual min. [N]	51.6	✓	51.9	✓	55.0	✓	54.6	✓
Max. uplift [mm]	45.1	x	45.0	x	46.8	x	46.6	x
Loss [%]	0	✓	0	✓	0	✓	0	✓

Table 5.3: Validation 300 km/h

	300 km/h							
	beam25		beam50		spr25		spr50	
F_M [N]	117.1	✓	117.4	✓	117.1	✓	117.1	✓
σ [N]	54.6	x	54.3	x	33.0	✓	33.0	✓
Stat. max. [N]	280.8	x	280.4	x	216.2	✓	216.1	✓
Stat. min. [N]	-46.7	x	-45.5	x	18.0	✓	18.1	✓
Actual max. [N]	272.9	x	273.2	x	194.3	✓	194.0	✓
Actual min. [N]	12.1	x	16.4	x	30.8	✓	30.4	✓
Max. uplift [mm]	53.4	x	49.5	x	54.9	x	54.8	x
Loss [%]	0	✓	0	✓	0	✓	0	✓

reality be rejected. However, the spring-damper dropper model is very close to being validated, only failing marginally at the support uplift. Thus, it is assumed that this model is able to replicate a catenary/pantograph interaction to some degree. The beam dropper model proves to be insufficiently accurate. It produces a large variation in force, where both maximum and minimum contact forces are way outside range. Figure 5.4 plots contact force against time for the two different models. It is evident that the contact force in the initial part of the graphs is irregular and disrupted. The explanation is that the pantograph experiences a sudden increase in velocity; from 0 to, in this case, 300 km/h. These large variations in contact force would most likely be eliminated if the train was given time to accelerate. However, the inclusion of a realistic train acceleration will blow up

the model size severely, leaving this option unrealistic. As an example, a train accelerating at 1 m/s^2 spends approximately 83 seconds, or 3.5 km, in the process of reaching 300 km/h. For the remaining part of the graph, the variation in contact force shows a clear periodic pattern, which is to be expected since the spans are identical.
The next step in the validation sequence would be to compare simulated values to real life measurements.

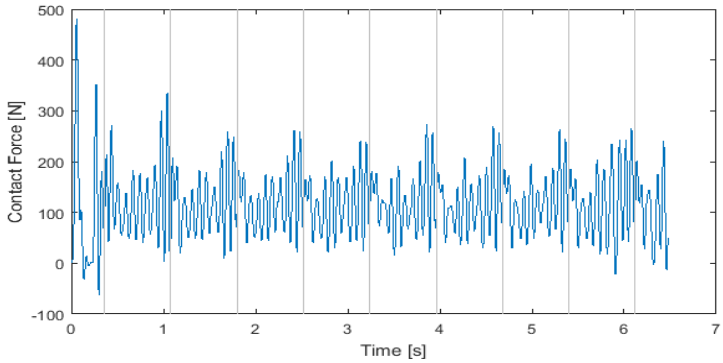

(a) Beam droppers, 0.5 m elements, 300 km/h, filtered at 20 Hz

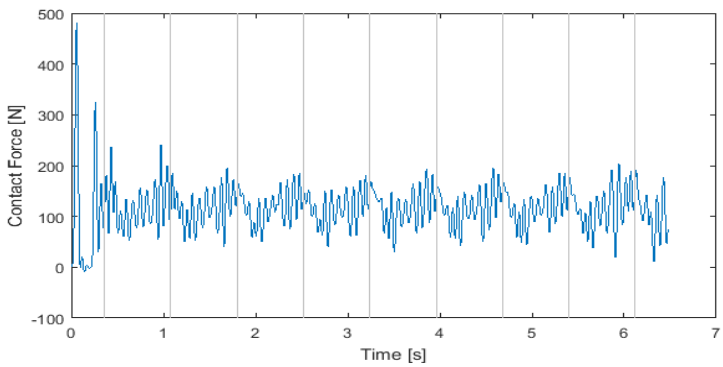

(b) Spring droppers, 0.5 m elements, 300 km/h, filtered at 20 Hz

Figure 5.4: Contact force plotted against time. Grey lines added at support location

5.5 Natural frequencies

Kiessling *et al.* presents an estimate for the fundamental frequencies of an OCL:

$$f_1 = \sqrt{\frac{H_{CW} + H_{CA}}{m'_{CW} + m'_{CA}}} \Big/ 2L \tag{5.1}$$

and

$$f_2 = \sqrt{\frac{H_{CW} + H_{CA}}{m'_{CW} + m'_{CA}}} \Big/ (2L + l_1) \tag{5.2}$$

where H and m' denotes tension and mass per meter, while L and l_1 are the span length and distance between the first field dropper and the support. (5.1) applies for non-symmetrical oscillations and (5.2) for symmetrical oscillations.
A simple modal analysis is performed to see if the natural frequencies from the model match these estimates. Three spans of 60 meters with 7 droppers per span are considered. The distance between the two droppers closest to the support, denoted l_1 in equation [5.2], is 4.5 meters. Both wires are applied a tension of 10 kN, and the total mass per meter is 1.39 kg. The resulting frequency estimates are $f_1 = 1.00Hz$ and $f_2 = 0.96Hz$.
Frequency extraction in ABAQUS returns the two modes presented in figure 5.5, with eigenfrequencies of 1.05 Hz and 0.98 Hz. The calculated eigenfrequencies

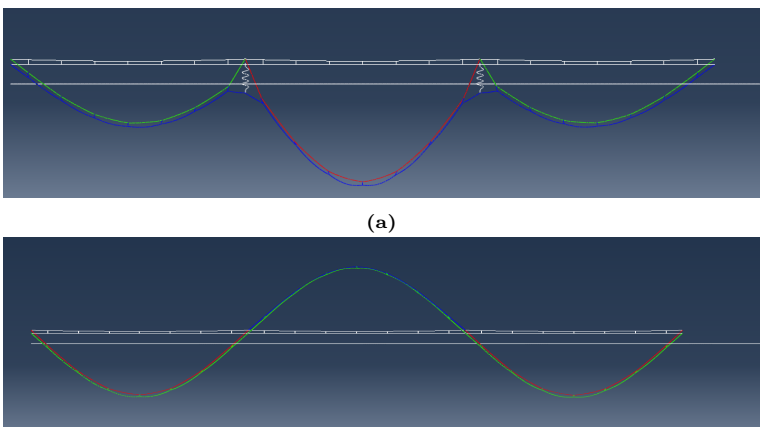

(a)

(b)

Figure 5.5: Eigenfrequencies and corresponding mode shapes (a): 0.98 Hz, (b): 1.05 Hz

show resemblance with the estimates, and the mode shapes also look as would be expected.
A complex eigenvalue extraction step is run to control how the applied Rayleigh damping is affecting the model. From this step, the effective damping ratio can be extracted directly. A plot relating the damping ratio to the frequencies is show in figure 5.6. The Rayleigh damping graph is added for comparison. It seems

as if the model is somewhat overdamped. The scatter plot actually follows the damping curve where the α-coefficient is set to two times its current value. The reason for this has not been found, but may be due to duplication somewhere in the script. The shape of the damping curve is as expected, and can be seen to be mass proportional in the examined range.

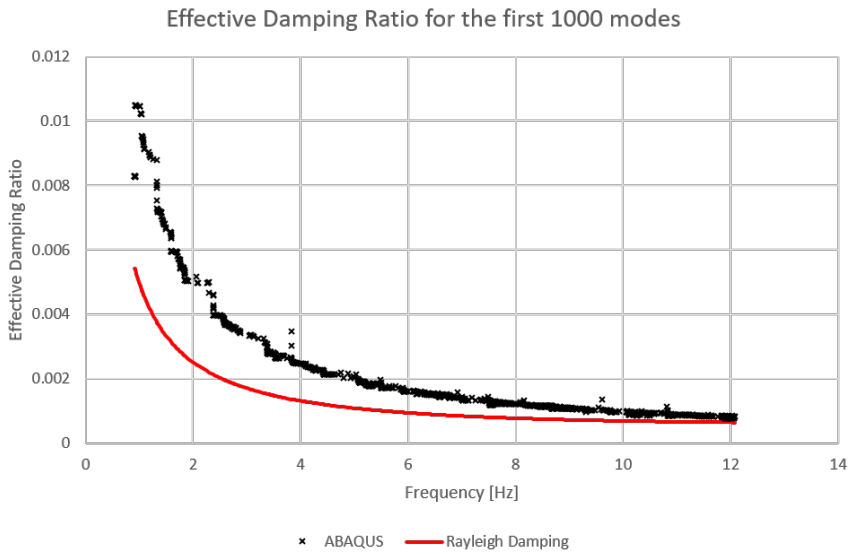

Figure 5.6: Effective damping ratio

5.6 Element length

In this section, the effect of element length alteration is studied. The lengths is altered for both the contact wire and catenary wire, whilst the droppers are unaffected, as they are modelled as springs. A track and catenary geometry similar to the one used in the validation process is considered, this time including span 3 to 7. Five different element lengths are tested, ranging from 0.05 meters to 1 m, and contact force parameters and time consumption is investigated. The results are rendered in figure 5.7. All in all, it seems as if the larger beam elements are able to produce approximately the same results as the smaller ones. Despite the 1m beams undershooting the contact force and maximum uplift compared to 0.05m beams, the variation is small, and considering the time consumption, they perform very well.

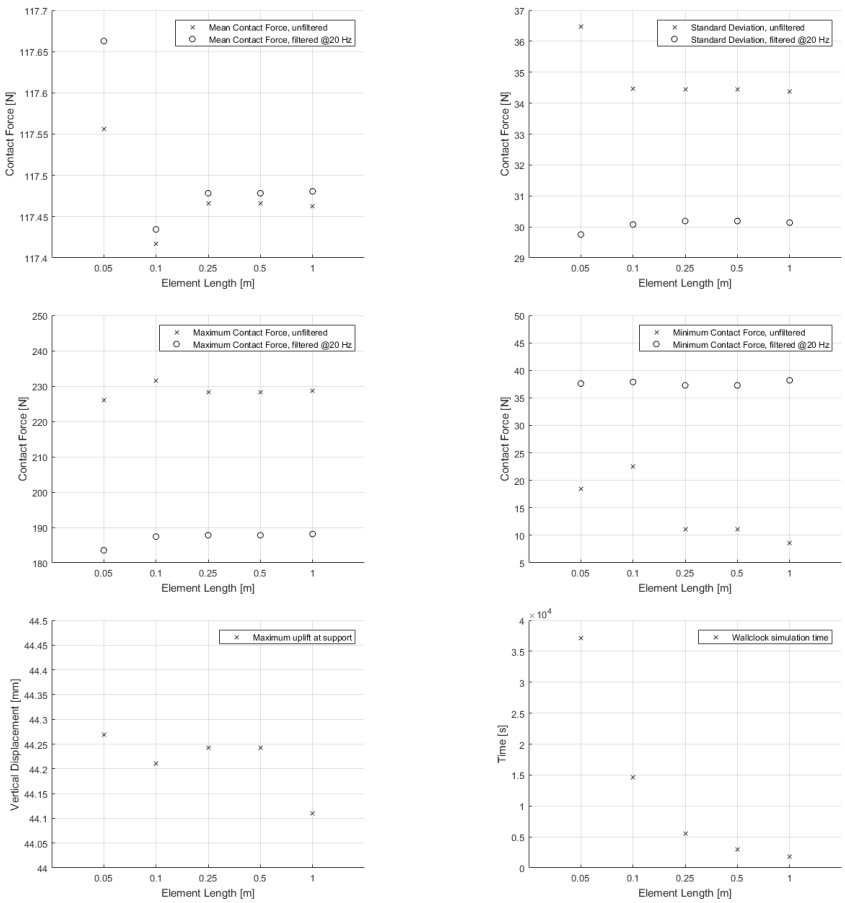

Figure 5.7: Effect of changing element size for both catenary wire and contact wire

5.7 Inclusion of cant height

As mentioned in section 2.4.1, stagger forces the contact wire to move from side to side, with a cyclic pattern, relative to the collector strips. The pantograph's working range limits the lateral motion. For a straight section, one full cycle is completed in two spans. For curved sections, on the other hand, the poles must be placed on the outside of the track, meaning that one cycle must be completed in only one span. The relative motion between contact wire and pantograph is also changed, since cant height is introduced in curves. Considering no pre-sag, the motion on a straight section will be purely in a horizontal plane. For a curve, however, lack of pre-sag causes variation in the contact forces, as the pantograph is slightly tilted. This is discussed by Rønnquist in [22], and depicted in figure 5.8. Thus, inclusion of pre-sag in the curves is believed to improve the performance of an OCL.

Figure 5.8: Stagger for straight (**a**) and curved (**b**) track. The tilt angle of the pantograph is exaggerated to highlight the difference.

The intention of this section is to examine the importance of including this cant height in the catenary model. Three generic tracks , each consisting of 14 40-meter spans of the system type Table 54 (with tension 10 kN/5 kN), are used throughout this study (figure 5.9). The first track is a straight section, the second includes a curve with a radius of 600 meters, while this curve radius is reduced to 300 meters in the last one. The curved track segments will be denoted R600 and R300. Travelling direction is towards the right in the figures, meaning that the curves are right curves. In a real life catenary section, a span length of 40 meters is generally not used for straight tracks segments. Dropper positions and lengths taken from appendix A therefore results in too much pre-sag and poorer performance. A more natural span length would have been 60 meters. The curved sections both contain clothoids of 80 meters into and out of the curve. A stagger of 0.4 meters is used, and for the curved tracks, the stagger is placed on the convex side of the track. Dropper positions and lengths are according to appendix A. The sections are run at three different speeds; 80, 110 and 140 km/h. These values are thus within a realistic scope for the chosen system, though in retrospect somewhat high regarding the sharp curves.

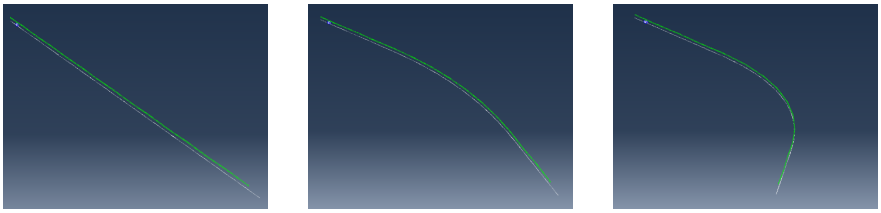

(a) R = ∞ **(b)** R = 600 m **(c)** R = 300 m

Figure 5.9: Track geometries

BaneNor's empirical equation

$$V = 0.291 \cdot \sqrt{R \cdot (h + I_{max})} \tag{5.3}$$

where

V = speed [km/h]
R = curvature [m]
h = cant height [mm]
I_{max} = limiting value for lack of cant height [mm]

relates the maximum speed allowed to the curvature and cant height. For 290 m $\leq$ R $\leq$ 600 m, I_{max} equals 130 mm [15], and a cant height of 150 mm in a curve with R = 300 m results in a maximum speed of 84.3 km/h. 140 km/h is therefore obviously an unrealistic value, but can still provide information on how response relates to speed. For the version with cant height, the values of this height has been set according to BaneNor's recommendations, tabulated in [7]. This means that the cant value depends on both the magnitude of curvature and speed. When the combination of small radius and high speed leads to cant height outside the permissible range, which is the case for R=300m/v=140km/h for example, the largest possible cant value is used.

5.7.1 Contact Force

When it comes to straight track geometry, the results will clearly be similar for a model including cant height and one that does not. However, it can be useful to have a benchmark. Figure 5.10 shows the contact force and its variation in the case of a straight track. Since identical spans are repeating over the whole segment, the contact forces vary in a smooth pattern. When curves are introduced, more variation is expected. The resulting contact force time series are presented in figure 5.11 and 5.12. A summary of all obtained key values is rendered in table 5.4.

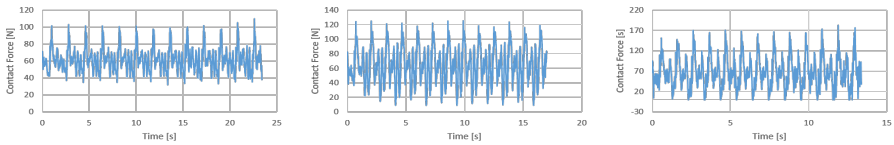

(a) v=80km/h **(b)** v=110km/h **(c)** v=140km/h

Figure 5.10: Time series, Straight

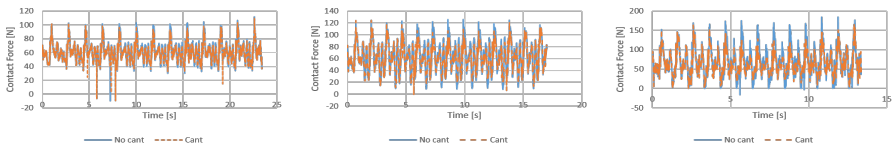

(a) v=80km/h, cant=52.5mm **(b)** v=110km/h, cant=110mm **(c)** v=140km/h, cant=150mm

Figure 5.11: Time series, R=600m

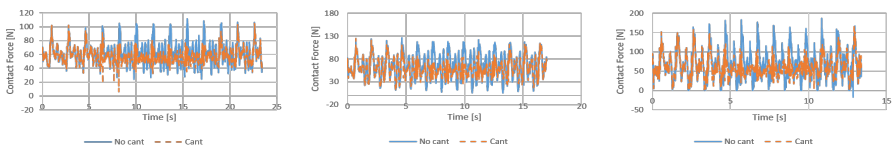

(a) v=80km/h, cant=125mm **(b)** v=110km/h, cant=150mm **(c)** v=140km/h, cant=150mm

Figure 5.12: Time series, R=300m

Variable	80 km/h	110 km/h	140 km/h
Straight, Mean CF [N]	60.8	63.6	67.0
R600 no cant, Mean CF [N]	60.8	63.7	67.0
R600 cant, Mean CF [N]	60.1	61.6	63.4
R300 no cant, Mean CF [N]	60.9	63.7	67.1
R300 cant, Mean CF [N]	57.5	58.4	59.7
Straight, St.dev. CF [N]	13.0	25.0	35.7
R600 no cant, St.dev. CF [N]	13.6	25.3	35.9
R600 cant, St.dev. CF [N]	12.1	21.4	27.8
R300 no cant, St.dev. CF [N]	15.1	26.2	36.0
R300 cant, St.dev. CF [N]	10.1	18.5	25.7
Straight, max. CF [N]	109.7	124.7	182.5
R600 no cant, max. CF [N]	111.8	125.3	183.7
R600 cant, max. CF [N]	109.3	124.3	163.4
R300 no cant, max. CF [N]	111.9	126.7	186.7
R300 cant, max. CF [N]	106.7	124.5	171.3
Straight, min. CF [N]	31.6	9.0	0
R600 no cant, min. CF [N]	-8.4	8.3	-16.2
R600 cant, min. CF [N]	-9.2	-1.4	0
R300 no cant, min. CF [N]	24.0	5.2	-17.2
R300 cant, min. CF [N]	5.9	12.9	0
Straight, max. supp. uplift [mm]	16.8	16.9	19.1
R600 no cant, max. supp. uplift [mm]	16.8	16.9	19.4
R600 cant, max. supp. uplift [mm]	16.6	16.9	17.2
R300 no cant, max. supp. uplift [mm]	16.9	16.9	21.2
R300 cant, max. supp. uplift [mm]	16.2	16.6	19.3

Table 5.4: Simulation results for the different tracks geometries

From the depicted time series, the effect of including cant height is observed. Compared to the straight section, the mean contact force for both R600 and R300 is higher or equal, and deviates slightly more, when the camber is set to zero. This applies to all the three speeds considered. Inclusion of cant height has the opposite effect, reducing both mean contact force and standard deviation. As the speed is increased, the effect becomes more and more apparent. Contact force reduction is probably because the displacement caused by the pre-sag harmonises well with the lateral movement relative to the contact strip. The lateral motion is affected by both cant height and curvature, which will be illustrated shortly. How the mean contact force and standard deviation of contact force changes with speed and curve radius, is presented in a more visual form in figure 5.13.
The maximum value of contact force follows the same pattern as the mean force and standard deviation, showing some reduction when cant height is included in the model. The minimum value, however, seems to be more random in nature. Since many of the values are actually negative, they are believed to be a result of a numerical error, maybe due to a rather coarse mesh. As the speed increases, this minimum value is close to zero for both cases, suggesting that this configuration's speed limit is exceeded.

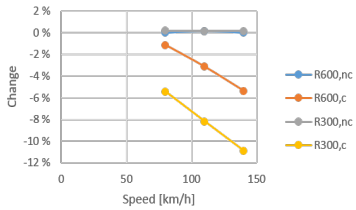

(a) Mean contact force change, straight section as reference

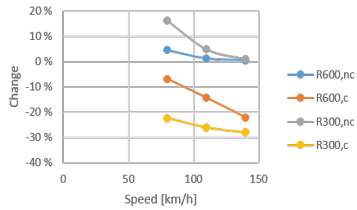

(b) Standard deviation of contact force change, straight section as reference

Figure 5.13

The running pantograph generates horizontal contact forces in addition to the vertical ones. Even when no cant is included, the stagger and pre-sag are responsible for the existence of these forces. When the pantograph is tilted through the curve, the magnitude of the contact force's horizontal component grows. Figure 5.14 shows the absolute value of the mentioned component for R300, 110 km/h. As expected, the canted version is seen to produce larger horizontal forces than the flat version, when passing through the curve. However, this contribution is not big enough to affect the total magnitude significantly.

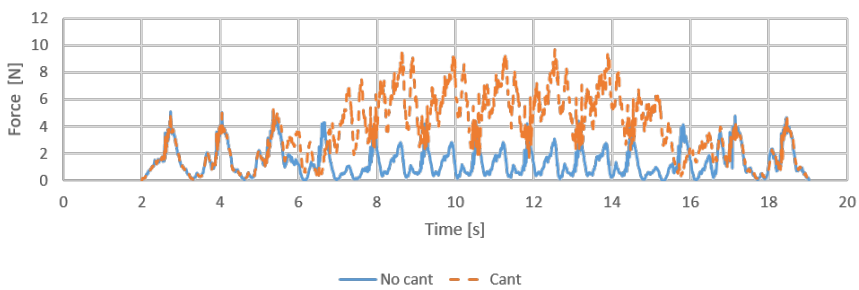

Figure 5.14: Horizontal forces present for R300, 110 km/h

5.7.2 Pantograph movement

The pantograph's vertical movement is traced along the section length. The relative displacements for R600 and R300 are shown in figure 5.15 and 5.16, respectively. A clear distinction between cant exclusion and inclusion can be observed. Firstly, the track elevation adds extra height to the pantograph reference point, as this is defined relative to the flat track. Also, where the pantograph in the model without cant height, experiences a smooth cyclic pattern, this is not the case when the cant height is included. When the pantograph hits the curve in the canted model of R300 at 80 km/h, the pantograph almost stops moving in vertical direction. Thus, it can be concluded that the magnitude of pre-sag combined with the curvature is somewhere near optimal. The trend of less movement with increasing cant height can be seen for R600 as well, however the height of 52.5 mm at 80 km/h seems to be too small to have a significant effect.
In figure 5.16, one can clearly see the impact of dynamic forces as the speed increases, and for the canted model, the pantograph experiences more movement.

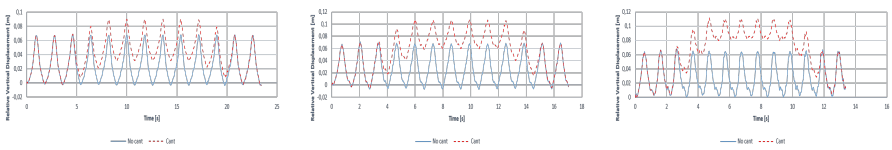

(a) v=80km/h, cant=52.5mm **(b)** v=110km/h, cant=110mm **(c)** v=140km/h, cant=150mm

Figure 5.15: Pantograph movement, R=600m

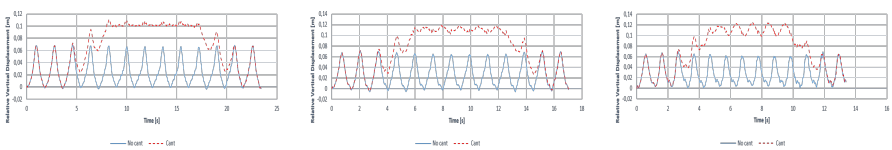

(a) v=80km/h, cant=125mm **(b)** v=110km/h, cant=150mm **(c)** v=140km/h, cant=150mm

Figure 5.16: Pantograph movement, R=300m

How the contact wire moves laterally on the collector strips is illustrated in figure 5.17. Here, a negative value corresponds to left when facing travelling direction. For the straight section, the contact wire moves from side to side in a zig-zag pattern, just as expected. The curves complicate the movement, and for R600 it is clear that only half of the pantograph's working area is being used. This is due to the span length not being fitted to the curve, and would in real life cause unnecessary wear in the long run. For R300, the span length is near optimal, allowing for a large proportion of the contact strips to be used, meaning also that more pre-sag is favourable compared to R600.

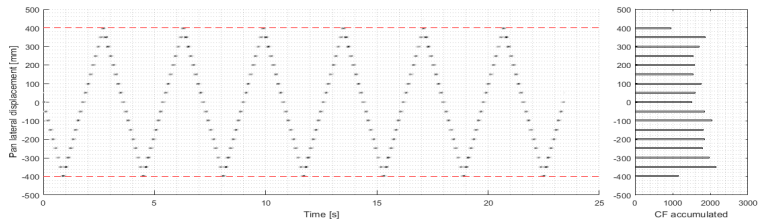

(a) Contact point position, R = ∞

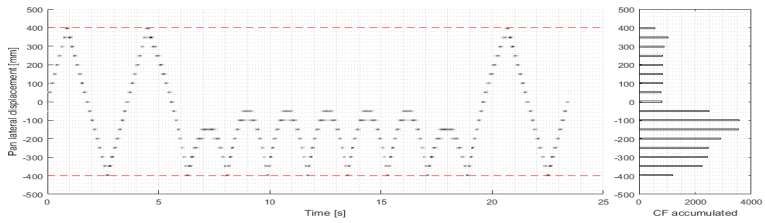

(b) Contact point position, R = 600

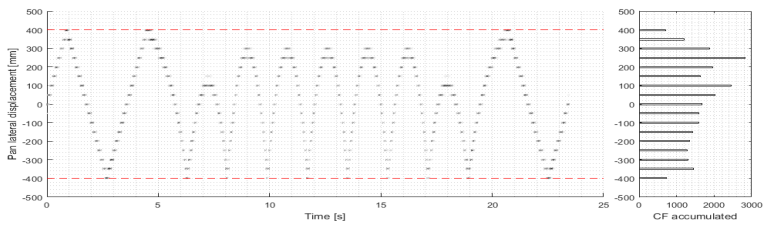

(c) Contact point position, R = 300

Figure 5.17: Lateral contact wire displacement relative to collector strips

5.7.3 Contact wire displacement

The contact wire uplift is examined for the sharpest curve, i.e. R300. Uplift data is extracted at the node where the contact wire is connected to pole number 8, which is approximately in the middle of the whole section. The resulting values are plotted against time in figure 5.18.

From these figures, the transverse wave moving at wave propagation speed is

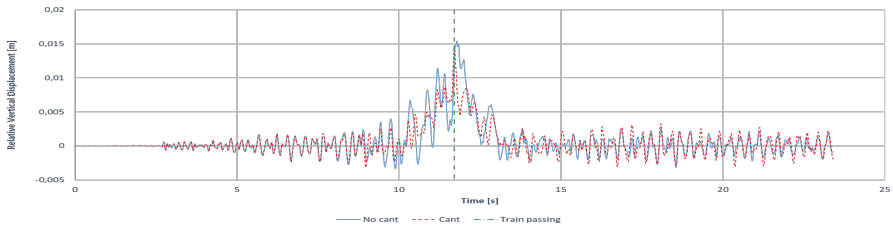

(a) R=300m, v=80km/h

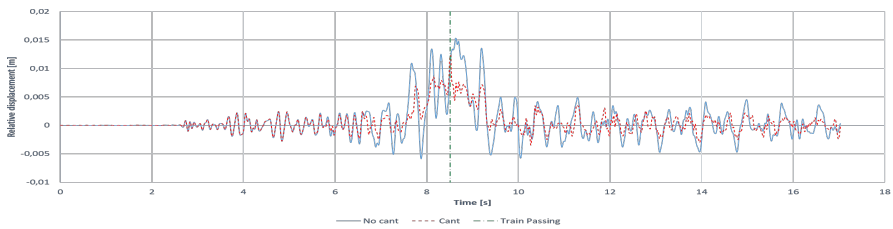

(b) R=300m, v=110km/h

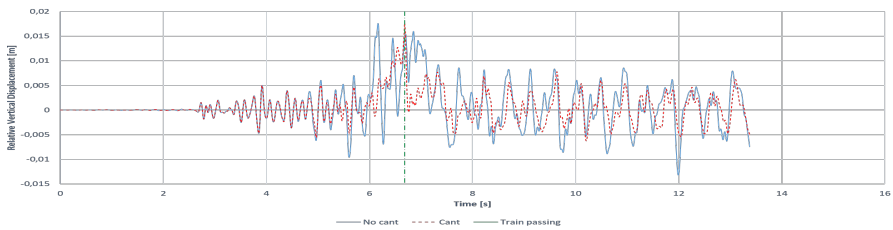

(c) R=300m, v=140km/h

Figure 5.18: Contact wire vertical displacement at pole 8

easily detected. With the point being 260 meters away from where the pantograph causes the first impulse, it should, according to theory, arrive at approximately $260\text{m}/\sqrt{10000\text{N}/0.93\text{kg/m}} = 2.51$ seconds. This is confirmed in all three plots. The difference between the canted model and the flat one seems to become more evident with increased speed. While the maximum uplift is approximately equal for both cases, the dynamic response, especially post-passage deviates to some degree. When running at 110 km/h and 140 km/h, the vibration amplitude of the canted version is slightly reduced compared to the version without cant. It can also be seen that the pre-passage response fluctuates less for the cant model. As expected,

the magnitude of vibration increases with speed in general.
Since the inclusion of cant height leads to a larger horizontal force component, it can be of interest to see how much the contact wire is displaced laterally. For a given configuration and a specified node, the displacement values in the global ABAQUS directions U1 and U3 are extracted. The node in query is located mid span between pole 7 and 8, and the radius and speed is 300 m and 110 km/h, respectively. The resulting graphs are plotted in figure 5.19. Since lateral movement is restricted by the steady-arm at each support, the resulting displacements are of relatively small magnitude. There is however a difference worth noticing, where the canted version almost doubles the displacement at train passage.

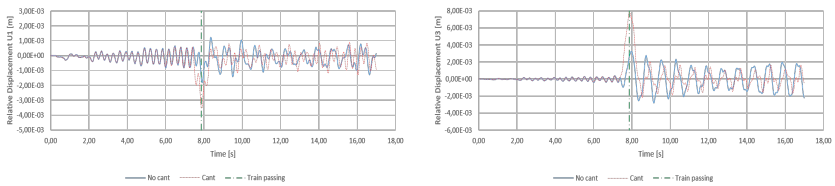

(a) Displacement global x-direction **(b)** Displacement global z-direction

Figure 5.19: Lateral displacement extracted for R=300m, v=110km/h. The node is located between pole 7 and 8.

5.8 Section Overlaps

This section aims to examine the effect of section overlaps. Several simulations are performed for a 10 span long catenary section, where each span is 60 meters and 9 droppers are placed per span. The reason for using this many droppers is simply because of an input error, that due to time limitation could not be fixed. For the same reason, the pre-sag is more uniform along the whole span than what should be the case. As can be seen from figure 5.20, the whole wire is lowered, while the use of tabulated dropper heights would have resulted in geometry similar to the one in figure 5.1.

Table 54 with contact wire tension of 10 kN and catenary wire tension of 5 kN

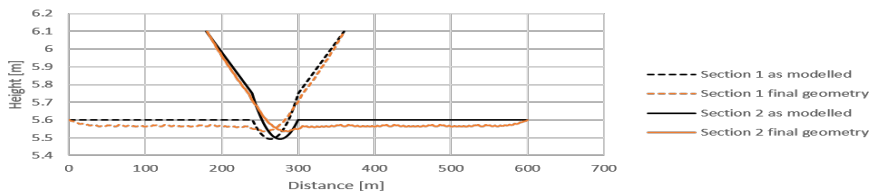

(a) Contact wire coordinates, overlapping mid span= -0.1m below CW height

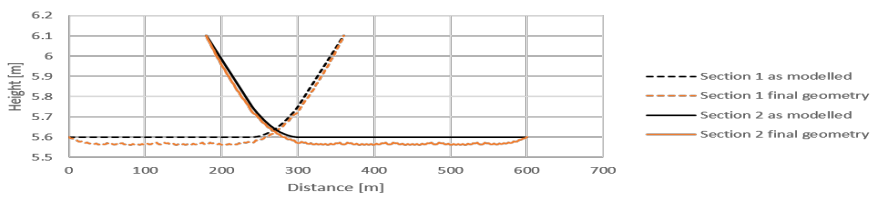

(b) Contact wire coordinates, overlapping mid span= 0.04m above CW height

Figure 5.20: Contact wire geometry before and after tension step

is used, leading to a pre-sag of approximately 4 cm mid span. If nothing else is specified, the overlapping section consist of three spans, where span 5 is the span where the pantograph for a short time is in contact with both contact wires. The contact wire geometry here is modelled similar to the overlap section seen in appendix A. Thus, the contact wire has a parabolic shape in the span where the overlap occurs. How the spans are modelled can also be seen in figure 5.20. The crossing point between the two wires is either raised or lowered when tension and gravity is applied, depending on the initial geometry.

The idea was to alter the variables speed, contact wire displacement at overlap's mid span, number of overlapping spans and distance between catenary systems when overlapping. Due to user errors, such as changing parameters for a proportion of the simulation runs, large parts of the results are deemed to be inconclusive, and thus the focus will be on the contact wire displacement at overlap's mid span. A plot showing differences between three and five overlap spans will also be included, however the number of data points is very limited.

5.8.1 Contact force

The overlapping span's initial mid span displacement is entered as a parameter ranging from -0.1 to 0.075 m, and the contact force and pantograph displacement is evaluated. The speed ranges from 100 to 160 km/h, in steps of 20 km/h. An illustration of how the contact is disturbed by overlap sections is provided in figure 5.21. The three different plots shows the contact force behaviour of a plain section with 10 identical spans, the same section with an overlap in span 5, and another section with overlap, but where the pre-sag is approximately 6 cm. Even though the effect of the overlapping spans can be observed in 5.21b, it is more chaotic and recognisable in 5.21c. It would therefore be interesting to perform more simulations for this case. All subsequent simulations are however performed with the pre-sag used in the second figure, due to the error mentioned earlier. Figure 5.22 shows mean contact force and standard deviation of contact force for span 2 to 9, while figure 5.23 focuses on the span where the pantograph connects with both contact wires.

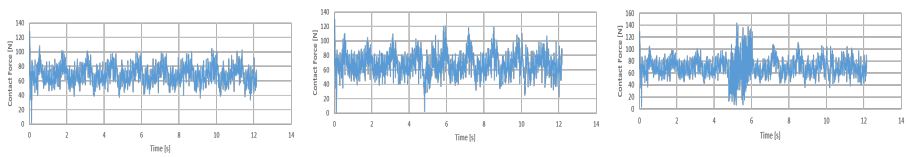

(a) No overlaps, v=160km/h **(b)** Overlap spans 3:5, v=160km/h **(c)** Overlap spans 3:5, v=160km/h

Figure 5.21: Time series for three different configurations

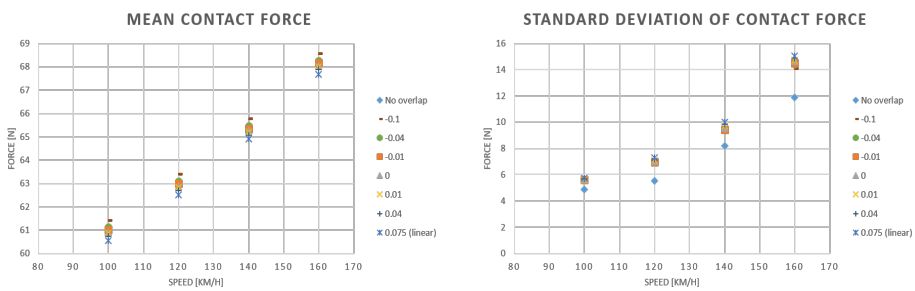

Figure 5.22: Data extracted for span 2 to 9

From figure 5.22, it can be observed that the mean contact force, when considering several span, is not affected to much degree. Compared to the case with no overlap, the standard deviation is slightly increased for all configurations. The impact of the overlapping span is also seen to increase with speed. When the

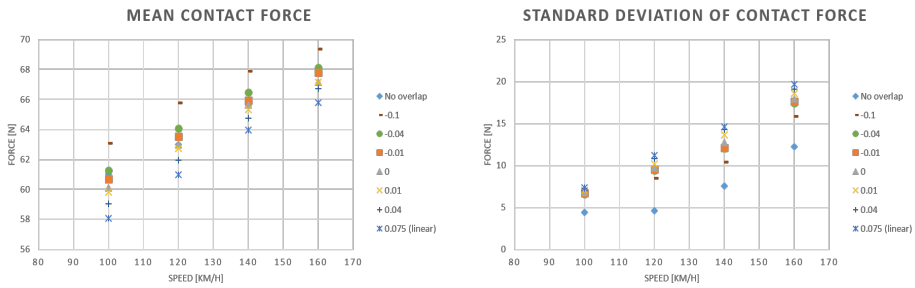

Figure 5.23: Data extracted for only span 5

overlapping span is isolated, the difference between the simulations becomes more evident. Still, the trends are similar, i.e. when the mid span is lifted, the mean contact force is reduced and the standard deviation of contact force is increased. This indicates that the "peak" value for negative initial displacement of the mid span is not reached. At some point, the amount of sag is expected to cause more disturbance, and rather an increase in standard deviation. It is ideal to have both a low contact force and standard deviation, ensuring low wear and small fluctuations, meaning that a compromise must be made.

Figure 5.24 attempts to explore the effect of using five overlap spans instead of

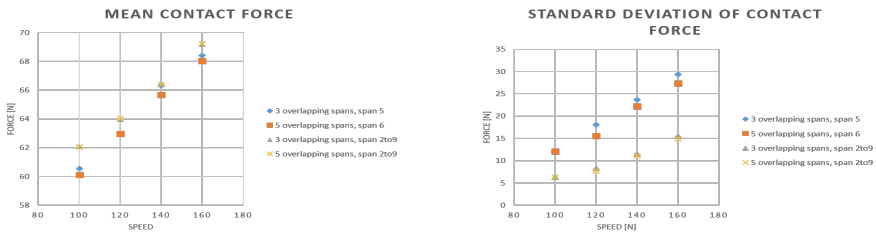

Figure 5.24: Effect of five overlap spans compared to three

three. The overlapping span is misplaced, and located in span 6, rather than 5. This is considered not to have too much impact. Also, this analysis was performed with more pre-sag than the ones shown so far. However, it is compared to a model with the same amount of sag, allowing for a fair comparison. The overlap span's mid span displacement was initially 0.04 m in upward direction.

The mean contact force is almost equal for the two cases, but the three-spanned version suffers from slightly higher forces. 120 km/h is an exception, where the magnitude is identical. Since the initial mid span point was lifted, it is not surprising that the force is reduces when only this span is considered. When it comes to the standard deviation, the five span overlap seems to perform better. This is in accordance with theory, because "hard" points on the contact line, such as fixed points, cause more disturbance, and the distance to this point is extended when using five spans.

5.8.2 Pantograph movement

The vertical pantograph movement is plotted for a crossing point 0.04 m above and 0.04 m below the contact wire height. Figure 5.25 renders the resulting displacements. From the figures, it can be concluded that the pantograph moves with the contact wire geometry, as expected. The originally lowered geometry is seen to cause less variation when the pantograph switches contact wire, but this does not affect movement post-passage. With the overlapping span ignored, the magnitude of displacement increases strongly with speed. As the speed increases, the presence of dynamic force becomes more evident, and the pantograph movement shifts from being disrupted to consisting of larger smooth waves.

Lateral contact wire movement relative to contact strips is plotted in figure 5.26.

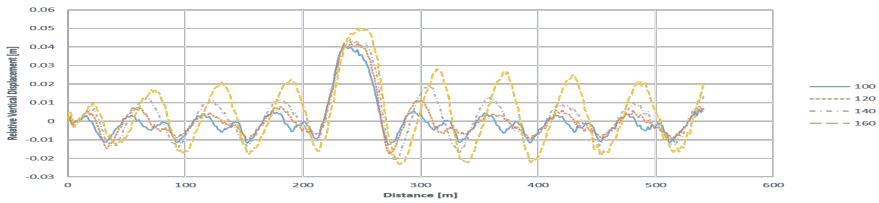

(a) Pantograph vertical movement, overlap mid span lifted 4 cm

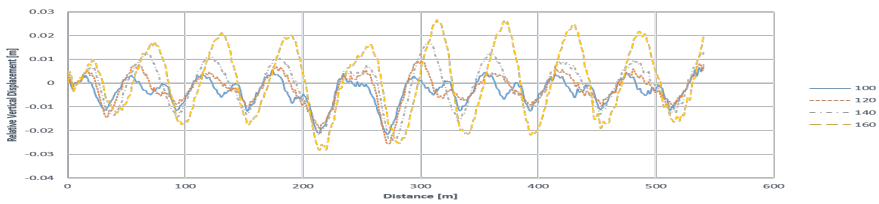

(b) Pantograph vertical movement, overlap mid span lowered 4 cm

Figure 5.25: Lateral contact wire displacement, v=100km/h

The figure illustrates the presence of two contact points at the same time. The distance between the two catenary systems is responsible for the shift in stagger. If the observed time period of contact is approximated to 0.5 seconds, this corresponds to about 14 meters for a train running at 100 km/h, which is the case here.

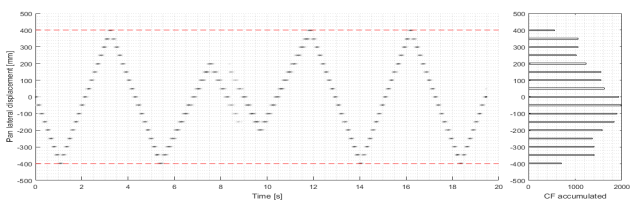

Figure 5.26: Lateral pantograph movement when passing an overlap section

Conclusion

Concluding remarks and suggestions for future work are presented in the following list:

- A functional numerical model with a large number of simulation variables has been created. The attempt to validate the model according to EN 50318 was unsuccessful, however by small margin.

- Controlling the tension and displacement values remains a big problem. Relatively small changes in the resulting geometry after adding tension and gravity, has proved to impact the output values. Controlling the contact wire displacement for generic catenary spans has turned out to be complicated, and has resulted in insufficient accuracy. Until the relationship between displacement, tensions, span lengths and droppers is resolved, the use of tabulated values is recommended.

- The model code is not to be considered as complete. It lacks a few important features, such as friction in pantograph, the ability to model several pantographs, gradually changing system height and contact wire height during a section, friction between pantograph and contact wire etc. The method for obtaining elasticity values should also be reconsidered. As the author is not very familiar with coding, the model code can also be considered as quite fragile. Parts of it may however be helpful for others attempting to develop similar codes.

- Including cant height in the numerical model has a significant effect on both contact force and displacement. The catenary system evaluated in this thesis included a rather large pre-sag, resulting in a force reduction, and also a reduction in vertical displacement of contact wire. Ideas for future work would include simulations through curves where the pre-sag is limited.

- The passing of an overlap section has shown to cause disturbance compared to a regular section. As the mid point of the overlapping span is raised, the mean contact force decreases while the standard deviation of contact force increases. Due to user error and time limitation, the study of overlapping spans was heavily reduced. Further exploration of the effects of passage is encouraged.

Appendix A

A.1 Overlap drawing including dimensions [6]

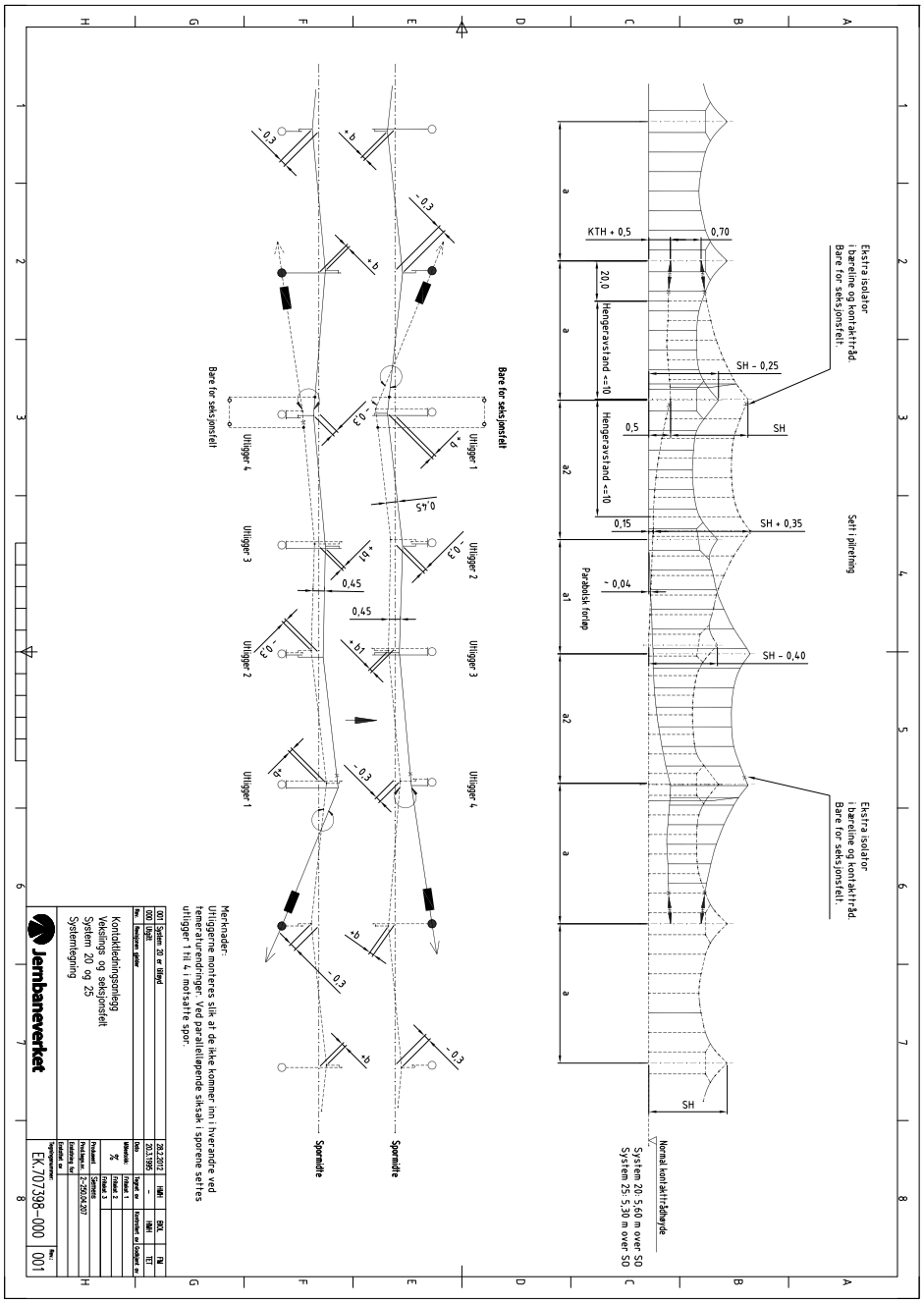

A.2 Dropper tables, pt.1 [14]

Nov. 1956

Hengetrådtabell for 100 mm² Kt og 80 mm² Kt med 50 mm² Bk for utliggerhöyder 2100, 1600, 280 og 215 mm. Tabell. nr 54

Ballansearm tegn 3909. Samlet strekk 1125 kg. Strömavtagertrykk 6 kg. Blad 2.

Strekkfordeling: 100 mm² Kt og 50 mm² Bk 625/500 kg. 80 mm² Kt og 50 mm² Bk 693/432 kg.

b) for utliggerhöyde 1600 mm.

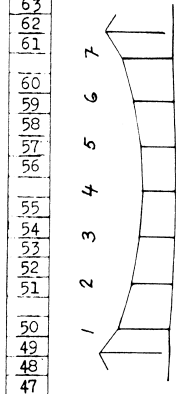

spennlengde	antall hengetråder	Hengetråd nr: 1 lengde	1 avst. fra utl.	2 lengde	2 avst. fra utl.	3 lengde	3 avst. fra utl.	4 lengde	4 avst. fra utl.	5 lengde	5 avst. fra utl.	6 lengde	6 avst. fra utl.	7 lengde	7 avst. fra utl.	nedheng ved midterste hengetråd(er) 100 mm²	80 mm²
m		cm	m	cm	m	cm	m	cm	m	cm	m	cm	m	cm	m	mm	mm
65		129	3,39	74	13,09	40	22,79	29	32,50	40	42,19	74	51,89	129	61,59	58	65
64		130	3,29	77	12,86	44	22,43	34	32,-	44	41,57	77	51,14	130	60,71	58	65
63		131	3,21	80	12,64	48	22,07	38	31,50	48	40,93	80	50,36	131	59,79	59	65
62		133	3,13	83	12,42	52	21,71	43	31,-	52	40,29	83	49,58	133	58,87	59	65
61		134	3,08	86	12,22	56	21,36	47	30,50	56	39,64	86	48,78	134	57,92	59	64
60		135	3,-	88	12,-	60	21,-	51	30,-	60	39,-	88	48,-	135	57,-	59	64
59		136	2,93	91	11,79	63	20,65	55	29,50	63	38,37	91	47,23	136	56,09	60	64
58		137	2,87	94	11,58	67	20,29	59	29,-	67	37,71	94	46,42	137	55,13	60	64
57		138	2,79	96	11,36	71	19,93	63	28,50	71	37,07	96	45,64	138	54,21	60	64
56		139	2,71	99	11,14	75	19,57	67	28,-	75	36,43	99	44,86	139	53,29	60	63
55		139	2,65	102	10,93	78	19,22	70	27,50	78	35,79	102	44,08	139	52,36	60	63
54		140	2,58	104	10,72	82	18,86	74	27,-	82	35,14	104	43,28	140	51,42	60	63
53		141	2,50	106	10,50	85	18,50	78	26,50	85	34,50	106	42,50	141	50,50	60	62
52		142	2,42	108	10,28	88	18,14	81	26,-	88	33,86	108	41,72	142	49,58	60	62
51		143	2,37	111	10,08	91	17,79	85	25,50	91	33,21	111	40,92	143	48,63	60	61
50		144	2,29	113	9,86	95	17,34	88	25,-	95	32,57	113	40,14	144	47,71	60	61
49		145	2,21	115	9,64	98	17,07	91	24,50	98	31,93	115	39,36	145	46,79	59	60
48		145	2,13	117	9,42	101	16,71	95	24,-	101	31,29	117	38,58	145	45,87	58	59
47		146	2,08	119	9,22	104	16,36	98	23,50	104	30,64	119	37,78	146	44,92	58	58
46		147	2,-	121	9,-	107	16,-	101	23,-	107	30,-	121	37,-	147	44,-	57	58
45		148	1,92	123	8,78	109	15,64	104	22,50	109	29,36	123	36,22	148	43,08	56	56
44		149	1,87	125	8,58	112	15,29	107	22,-	112	28,71	125	35,42	149	42,13	55	55

Se grafisk hengetrådtabell nr. 58 bl. 1.

A.3 Dropper tables, pt.2 [14]

Rettet 10.10.80

Hengetrådtabell for 100 mm² og 80 mm² Kt med 50 mm² Bk for utliggerhöyder 2100, 1600, 280 og 215 mm.

Tabell nr 54
Blad nr 3.

Ballansearm tegn 3909. Samlet strekk 1125 kg. Strömavtagertrykk 6 kg.

Strekkfordeling: loo mm² Kt og 50 mm² Bk 625/500 kg. 80 mm² Kt og 50 mm² Bk 693/432 kg.

b) for utliggerhöyde 1600 mm (forts.)

spennlengde	antall hengetråder	Hengetråd nr: 1 lengde	1 avst. fra utl.	2 lengde	2 avst. fra utl.	3 lengde	3 avst. fra utl.	4 lengde	4 avst. fra utl.	5 lengde	5 avst. fra utl.	6 lengde	6 avst. fra utl.	nedheng ved midterste hengetråd(er) 100 mm²	80 mm²	Anm.
m		cm	m	cm	m	cm	m	cm	m	cm	m	cm	m	mm	mm	
43	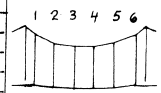	146	2,33	123	10,-	109	17,67	109	25,34	123	33,01	146	40,68	50	48	Gradish henge-tråd-tabell nr. 58 bl. 2
42		147	2,25	125	9,75	112	17,25	112	24,75	125	32,25	147	39,75	50	48	
41		148	2,18	127	9,51	115	16,84	115	24,17	127	31,50	148	38,83	49	47	
40		148	2,08	129	9,25	118	16,42	118	23,59	129	30,76	148	37,93	48	47	
39		149	2,-	130	9,-	120	16,-	120	23,-	130	30,-	149	37,-	47	46	
38		150	1,93	132	8,76	123	15,59	123	22,42	132	29,25	150	36,08	46	45	
37	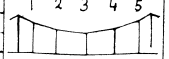	147	2,50	129	10,50	123	18,50	129	26,50	147	34,50			44	42	nr. 58 bl. 3
36		148	2,40	131	10,20	125	18,-	131	25,80	148	33,60			44	42	
35		149	2,30	133	9,90	127	17,50	133	25,10	149	32,70			44	41	-»-
34		150	2,20	135	9,60	129	17,-	135	24,40	150	31,80			43	41	
33	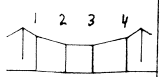	146	3,-	132	12,-	132	21,-	146	30,-					33	31	
32		147	2,88	135	11,63	135	20,38	148	29,13					33	31	nr. 58 bl. 4
31		148	2,75	137	11,25	137	19,75	148	28,25					32	30	
30		149	2,63	139	10,88	139	19,13	149	27,38					32	30	-»-
29		150	2,50	140	10,50	140	18,50	150	28,50					31	30	
28		151	2,38	142	10,13	142	17,88	151	25,63					31	29	
27	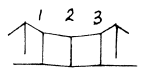	147	3,50	140	13,50	147	23,50							29	27	
26		148	3,33	142	13,-	148	22,67							29	27	
25		149	3,17	144	12,50	149	21,83							29	27	nr. 58 bl. 5
24		150	3,-	146	12,-	150	21,-							28	26	-»-
23		151	2,83	148	11,50	151	20,17							28	25	
22		152	2,67	149	11,-	152	19,33							27	25	
21		153	2,50	150	10,50	153	18,50							26	24	
20		154	2,33	151	10,-	154	17,67							25	23	

20)

Bibliography

[1] Collina A. and Bruni S. "Numerical Simulation of Pantograph-Overhead Equipment Interaction". In: *Vehicle System Dynamics* 38.4 (2002), pp. 261–291. DOI: https://doi.org/10.1076/vesd.38.4.261.8286.

[2] Rønnquist A. and Nåvik P. "Dynamic assessment of existing soft catenary systems using modal analysis to explore higher train velocities: a case study of a Norwegian contact line system". In: *Vehicle System Dynamics* 53.6 (2015), pp. 756–774. DOI: https://doi.org/10.1080/00423114.2015.1013040.

[3] Ambósio J. A. C., Pombo J., Pereira M. and Mósca A. "A computational procedure for the dynamic analysis of the catenary-pantograph interaction in high-speed trains". In: *Journal of Theoretical and Applied Mechanics* 50.3 (2012), pp. 681–699.

[4] Ambrósio J., Rauter F., Pombo J. and Pereira M. S. "A Flexible Multibody Pantograph Model for the Analysis of the Catenary–Pantograph Contact". In: *Multibody Dynamics*. Ed. by Arczewski K., Blajer W., Fraczek J. and Wojtyra M. Springer, 2011, pp. 1–27. ISBN: 978-90-481-9971-6.

[5] BaneNor. *BaneNor. 2017. Kontaktledning/ Prosjektering og Bygging/ Kontraktledningsutforming*
. URL: https://trv.banenor.no/wiki/Kontaktledning/%20Prosjektering_og_Bygging/Kontaktledningsutforming. (accessed: 09.04.2018).

[6] BaneNor/JBV. *Kontaktledningsanlegg, Vekslings- og seksjonsfelt, System 20 og 25, Systemtegning*. URL: http://www.banenor.no/elkraft/kl/sp.htm. (accessed: 25.04.2018).

[7] BaneNor/JBV. *Traseringstabeller for eksisterende baner*. URL: https://trv.banenor.no/wiki/Overbygning/Prosjektering/Sporets_tras%5C%C3%5C%A9/Vedlegg/Traseringstabeller_for_eksisterende_baner. (accessed: 30.04.2018).

[8] Cook R. D., Malkus D. S., Plesha M. E. and Witt R. J. *Concepts and Application of Finite Element Analysis*. John Wiley & Sons, 2001. ISBN: 978-0-471-35605-9.

[9] Dahlberg T. "Moving force on an axially loaded beam—with applications to a railway overhead contact wire". In: *Vehicle System Dynamics* 44.8 (2006), pp. 631–644. DOI: https://doi.org/10.1080/00423110500165523.

[10] Drugge L., Larsson T. C. and Stensson A. "Modelling and simulation of catenary-pantograph interaction". In: *Vehicle System Dynamics* 33 (2000), p. 490.501.

[11] *"Validation of simulation of the dynamic interaction between pantograph and overhead contact line"*. Standard. Brussels, BE: European Comitee for Electrotechnical Standardization, July 2002.

[12] Cho Y. H. "Numerical simulation of the dynamic responses of railway overhead contact lines to a moving pantograph, considering a nonlinear dropper". In: *Journal of Sound and Vibration* 315.3 (2008), pp. 433–454. DOI: https://doi.org/10.1016/j.jsv.2008.02.024.

[13] Hilber H. M., Hughes T.J.R. and Taylor R. L. "Improved numerical dissipation for time integration algorithms in structural dynamics". In: *Earthquake Engineering and Structural Dynamics* 5.3 (1977), pp. 283–292. DOI: https://doi.org/10.1002/eqe.4290050306.

[14] *"Kontaktledning: Regler for Prosjektering"*. Standard. Jernbaneverket, Feb. 2005.

[15] Jernbanekompetanse. *Sporets trasé/ Sporgeometri* . URL: http://www.jernbanekompetanse.no/wiki/Sporets_tras%5C%C3%5C%A9/Sporgeometri. (accessed: 30.04.2018).

[16] Kiessling and Puschmann and Schmieder and Schneider. *Contact Lines for Electric Railways, 2. edition.* Publicis Publishing, 2009. ISBN: 9783895783227.

[17] Luo R., Zeng J. and Zhang W. "Pantograph Dynamics and Control of Tilting Train". In: *IFAC Proceedings Volumes* 41.2 (2008), pp. 8293–8298. DOI: https://doi.org/10.3182/20080706-5-KR-1001.01402.

[18] Nåvik P., Rønnquist A. and Stichel S. "Identification of system damping in railway catenary wire systems from full-scale measurements". In: *Engineering Structures* 113 (2016), pp. 71–78. DOI: https://doi.org/10.1016/j.engstruct.2016.01.031.

[19] Nåvik P., Rønnquist A. and Stichel S. "Variation in predicting pantograph – catenary interaction contact forces, numerical simulations and field measurements". In: *Vehicle System Dynamics* 55.9 (2017), pp. 1265–1282. DOI: https://doi.org/10.1080/00423114.2017.1308523.

[20] Poetch G., Evans J., Meisinger R., Kortüm W., Baldauf W., Veitl A. and Wallaschek J. "Pantograph/Catenary Dynamics and Control". In: *Vehicle System Dynamics* 28 (1997), pp. 159–195. DOI: https://doi.org/10.1080/00423119708969353.

[21] Qian W. J., Chen G. X., Zhang W. H., Ouyang H. and Zhou Z. R. "Friction-Induced, Self-Excited Vibration of a Pantograph-Catenary System". In: *Journal of Vibration and Acoustics* 135.5 (2013), p. 051021. DOI: 10.1115/1.4023999.

[22] Rønnquist A. and Nåvik P. "Dynamic implications for higher speed in sharp curves of an existing Norwegian overhead contact line system for electric railways". In: *Proceedings of the 9th International Conference on Structural Dynamics, EURODYN 2014* (2014).

[23] Saltelli A., Ratto M., Andres T., Campolongo F., Cariboni J., Gatelli D., Saisana M. and Tarantola S. *Global Sensitivity Analysis, The Primer*. John Wiley & Sons, 2008. ISBN: 978-0-470-05997-5.

[24] Seo J.H., Kim S.W., Jung I.H., Park T.W., Mok J.Y., Kim Y. G. and Chai J. B. "Dynamic analysis of a pantograph–catenary system using absolute nodal coordinates". In: *Vehicle System Dynamics* 44.8 (2006), pp. 615–630. DOI: `https://doi.org/10.1080/00423110500373721`.

[25] Song Y., Liu Z., Wang H., Lu X. and Zhang J. "Nonlinear modelling of high-speed catenary based on analytical expressions of cable and truss elements". In: *Vehicle System Dynamics* 53.10 (2015), pp. 1455–1479. DOI: `https://doi.org/10.1080/00423114.2015.1051548`.

[26] Dassault Systemes. "ABAQUS 6.14 Analysis User Guide". In: 2014.

[27] Dassault Systemes. "ABAQUS 6.14 Keywords Reference Guide". In: 2014.

[28] Dassault Systemes. "ABAQUS 6.14 Scripting Reference Guide". In: 2014.

[29] Dassault Systemes. "ABAQUS 6.14 Theory Guide". In: 2014.

[30] TSI. *(2008/284/CE),L104,4.2.12*. Commission Decision/Directive. Technical Specifications for Interoperability, 2008.

[31] Zhang W., Liu Y. and Mei G. "Evaluation of the coupled dynamical response of a pantograph – catenary system: contact force and stresses". In: *Vehicle System Dynamics* 44.8 (2006), pp. 645–658. DOI: `https://doi.org/10.1080/00423110600744656`.